A Simulation of the Winter and Summer Circulations with the NMC Global Spectral Model

J. L. KINTER, III, J. SHUKLA, L. MARX AND E. K. SCHNEIDER

Center for Ocean–Land–Atmosphere Interactions, Department of Meteorology, University of Maryland, College Park, Maryland

(Manuscript received 20 May 1987, in final form 18 November 1987)

ABSTRACT

The medium range forecast model of the National Meteorological Center (NMC) has been integrated to produce winter and summer simulations. For the winter simulation, the model was initialized with the NMC analysis of 1200 UTC 15 December 1985 and integrated for 110 days to simulate the December–March period (referred to hereinafter as the DJFM simulation). For the summer simulation, the model was initialized with NMC analysis of 0000 UTC 1 May 1986 and was integrated for 110 days to simulate the May–August period (MJJA simulation). In each case, seasonally varying boundary conditions of sea surface temperature, soil moisture and sea ice were used. The computer code used was nearly identical to that used by NMC for the operational ten-day forecast during the period 16 April 1985 through 30 May 1986. Both simulations have been compared to the NMC analyses for the corresponding period.

It was found that the model climatology, defined as the average over the last 3 months of each run, is similar to that of the observed atmosphere as well as climatologies of other general circulation models. Notably, the model maintains a reasonable horizontal temperature gradient and circulation distribution, but the model is colder than observed in the troposphere nearly everywhere and cools in the lower stratosphere in the tropics and near the poles in both simulations. A detailed description of the stationary and transient features of the model circulation including both tropical and extratropical regions is also given. In addition, the model hydrological cycle, radiative balance and surface heat budget are discussed. The secondary circulations in the tropics including the zonally symmetric Hadley cell, as simulated by the model, are also compared with the observations. The upper branch of the Hadley cell appears to be only poorly simulated in DJFM.

Generally, the simulations demonstrated reasonable agreement with the observations in sea level pressure, the structure of the tropospheric zonal jets and the winter hemispheric stationary waves. The tropical rainfall is very different from climatology or surrogates for precipitation observations—such as outgoing long radiation—particularly in the excessive amount of rain produced by the model over subtropical deserts. The summer hemisphere in both simulations does not agree with observations as well as the winter hemisphere; this may be related to the tropical rainfall problem.

1. Introduction

In any assessment or verification of a numerical weather prediction model, the question of climate drift, the deviation of the long-term time mean of the model from the observed climatology for a given season, becomes important if forecasts longer than a few days are to be used. For this reason, it is important to compute and analyze the time mean of the model in conjunction with the production of extended range forecasts. As part of the Dynamical Extended Range Forecasting (DERF) Project at the National Meteorological Center (NMC), the operational global weather prediction model has been and will be integrated for periods of 30 days and more on a quasi-regular experimental basis. In order to understand the results of these integrations better and to diagnose the properties of the NMC operational model, we have computed the model's seasonal mean for both 15 December–15 March (DJFM) and 1 May–31 August (MJJA) by integrating the model for two entire seasons.

Our goal is to understand the role of atmosphere–ocean and atmosphere–land interactions in the variability and predictability of monthly and seasonally averaged atmospheric circulation. In order to carry out sensitivity and predictability studies toward this goal, we have chosen to utilize a model which is very similar to the one used operationally by NMC. This will enable us to compare the long-term simulations with the medium range (0–10 days) forecasts which are routinely produced by NMC.

In the past, several modeling groups have performed similar integrations of their respective general circulation models (GCMs). In those studies, a great emphasis was generally placed on the models' ability to reproduce the observed distribution of stationary waves and transient eddies, particularly in the extratropics. We will also examine the behavior of the NMC me-

Corresponding author address: Dr. James L. Kinter III, Center for Ocean–Land–Atmosphere Interactions, Dept. of Meteorology, University of Maryland, College Park, MD 20742.

dium range forecast model in that fashion, and we will give greater emphasis to the tropical circulation which, although difficult to verify, may be just as important in affecting global weather.

The present study is different from previous investigations in two important respects. First, we have used the operational forecast model which is used to routinely produce 10-day forecasts as well as to produce global datasets (NMC analyses) which are used by the research community for a variety of synoptic and diagnostic studies. Second, we compare the model simulations with the global NMC analyses for the (Northern Hemisphere) winter season of 1985–86 and the summer season of 1986 rather than the long-term climatology.

In the sections that follow, a description of the model and its simulated winter and summer circulations will be presented. Section 2 is a short description of the technical aspects of the model, and the model's boundary conditions and fixed fields are described in section 3. The time mean circulation in both the tropics and the extratropics is discussed in section 4. Section 5 is a description of the stationary wave behavior and transient eddies in the model as compared with the observations. The model's moisture budget and surface heat fluxes are described in section 6. Finally, some concluding remarks are given in section 7.

2. Description of the model and experimental design

The model used in this investigation is the operational, global spectral model of the National Meteorological Center which is an updated and improved version of the model described by Sela (1980). Model predictions employ the primitive equations of motion and a prognostic equation for the mixing ratio of water vapor. The vertical and horizontal structure of the variables in the equations are separated and discretized independently. The vertical derivatives are written in centered difference form using a modified sigma (normalized pressure) vertical coordinate (Phillips 1957), with 18 levels, equally spaced in sigma. The horizontal parts of all prognostic variables are expressed as coefficients of projection on the spherical harmonics, the eigenvalues of the spherical Laplacian operator. Nonlinear terms in the hydrodynamic equations, which are quadratic products of prognostic variables according to the form of the advection operator, are computed by the spectral transform technique (Orszag 1970) with rhomboidal truncation at wave number 40. The difference equations are then integrated forward in time using a semi-implicit scheme (Robert et al. 1972).

The parameterization of subgrid scale physical processes is adapted from the E2 physics from GFDL (Miyakoda and Sirutis 1977). The physics includes a parameterization for the absorption of solar radiation (Lacis and Hansen 1974), a radiative transfer calculation for the longwave components of terrestrial radiation (Fels and Schwarzkopf 1975; Fels and Schwarzkopf 1981), a boundary layer momentum and heat flux parameterization based on the mixing length theory of Monin and Obukhov (1954), a three-layer soil temperature formulation for the surface heat balance (Miyakoda and Sirutis 1977), a ground hydrology budget for soil moisture (after Manabe 1969) and a modified Kuo scheme for convection (Sela 1980; after Kuo 1965; and Phillips 1979). Momentum, heat and moisture are diffused horizontally on constant sigma surfaces by means of a biharmonic diffusion (Laplacian-squared) operator. Additionally, momentum and moisture are diffused vertically using a diffusion coefficient which is static stability dependent. The basis for the inclusion of these parameterizations into the model is described in more detail in Miyakoda and Sirutis (1986).

The model is initialized using a two-iteration, nonlinear normal mode scheme (Machenauer 1977) in which model generated diabatic heating is included. For the DJFM simulation, the model was run from observed initial conditions taken from 15 December 1985 at 1200 UTC, and for MJJA, 1 May 1986 at 0000 UTC was used. The boundary conditions used were climatological, seasonally varying surface conditions derived from a number of recently available sources (see section 3 for details). The radiative transfer calculation included specified, zonally symmetric cloudiness and ozone mixing ratio derived from observed seasonal mean values as used in the operational model. The model was integrated through 31 March 1986 in DJFM and 31 August 1986 for MJJA.

The two simulations were made using the same model which was used to produce global, 10-day forecasts each day at NMC during the corresponding period except for three differences. First, the operational model boundary conditions are taken from operational analyses of surface conditions to the extent available; surface conditions which are not available at the initial time are set to climatological values. These boundary conditions are then fixed for the 10-day integration of the forecast. In contrast, we used a climatological dataset and included a representation of the seasonal cycle of the boundary conditions. The impact of including the seasonal variation of the boundary conditions will be discussed in a later paper in which a comparison to an otherwise identical integration with fixed boundary conditions is made. Second, soil moisture evolved according to a bucket hydrology in the operational model, while we reset the soil moisture to its climatological value at the beginning of each model day. Third, in using the Fels–Schwartzkopf radiative transfer parameterization, the operational model incorporated a vertical interpolation from its own sigma levels to the GFDL model sigmal levels. We modified this interpolation by setting the top GFDL sigma level temperature equal to the temperature of the layer below it to avoid upward extrapolation since the upward extrap-

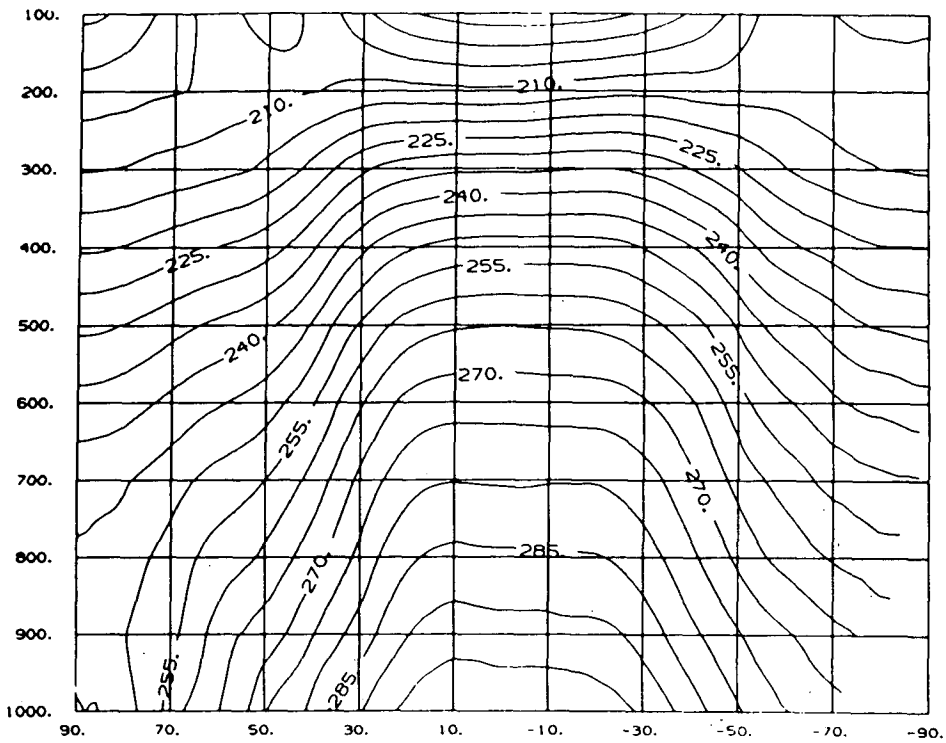

FIG. 4.1a. The DJFM mean of the simulated zonal mean temperature. The North Pole is at the left edge, and the South Pole is at the right edge. The ordinate is linear in pressure with 1000 mb at the bottom and 100 mb at the top. The contour interval is 5 K.

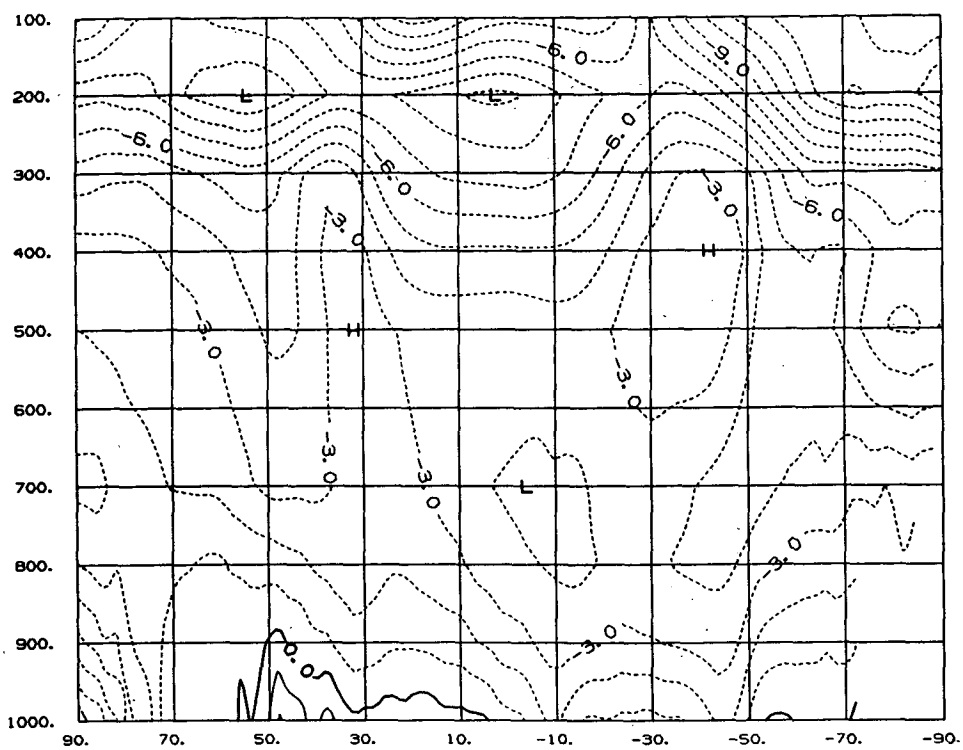

FIG. 4.1b. The DJFM mean of the zonal mean temperature error (simulation minus analyses). The contour interval is 1 K. Dashed contours are negative.

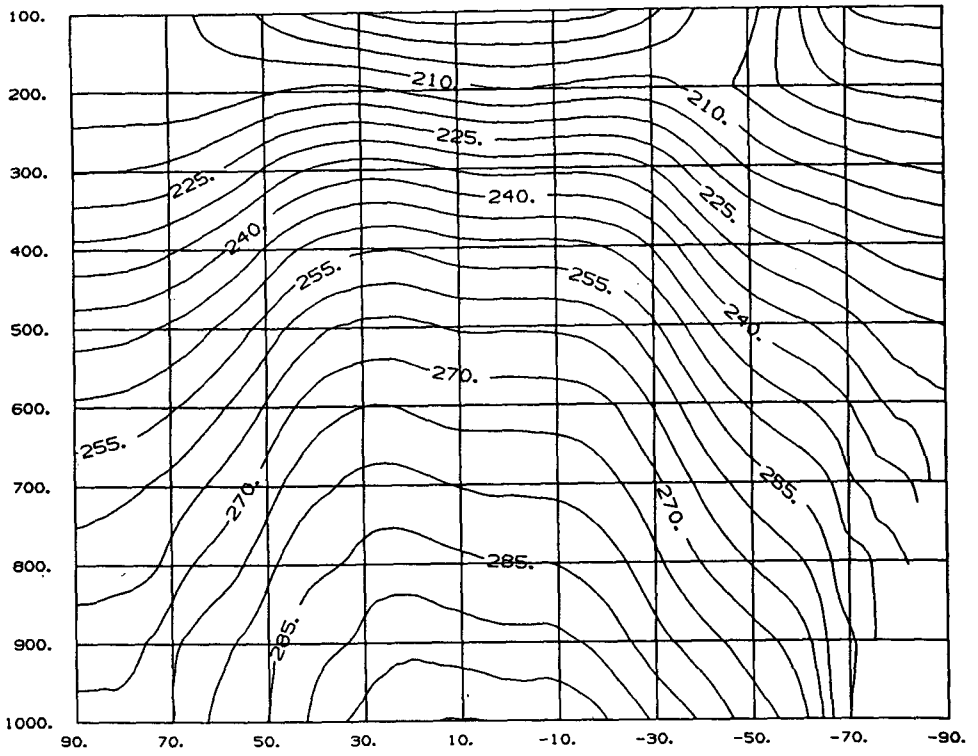

FIG. 4.2a. The MJJA mean of the simulated zonal mean temperature. The contour interval is 5 K.

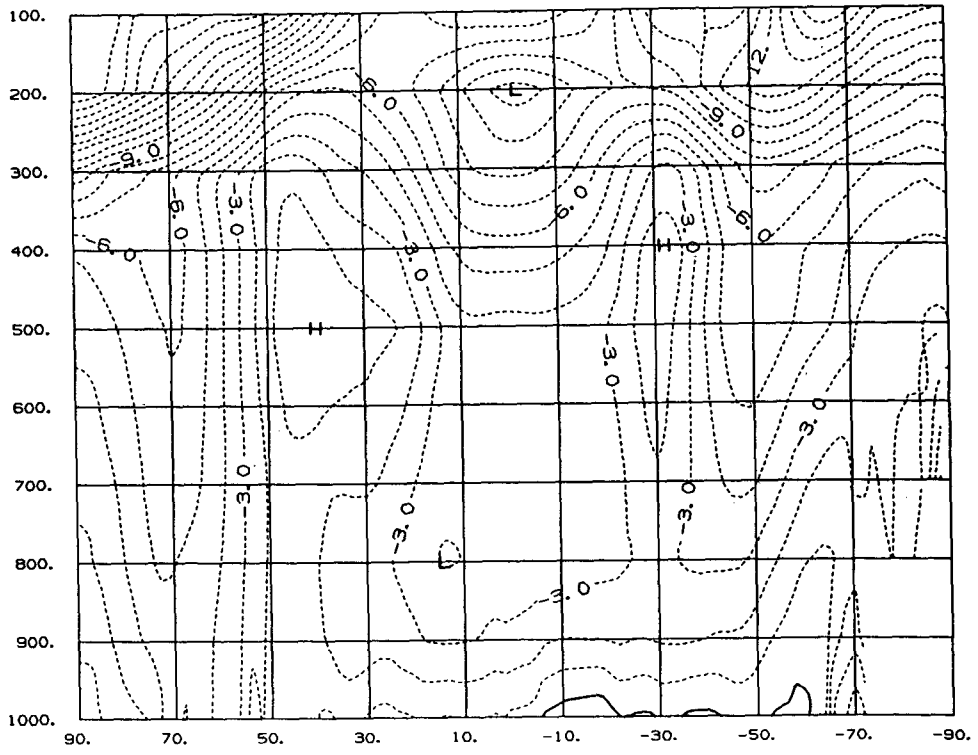

FIG. 4.2b. The MJJA mean of the zonal mean temperature error. The contour interval is 1 K. Dashed contours are negative.

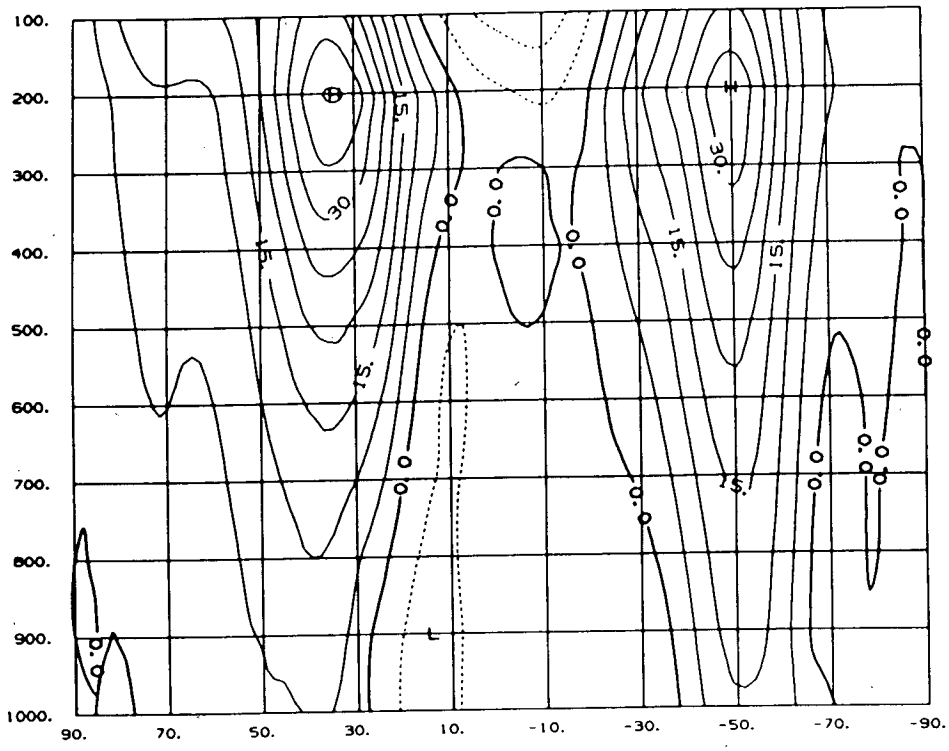

FIG. 4.3a. The DJFM mean of the simulated zonal mean zonal wind. The contour interval is 5 m s^{-1}. Dashed contours are negative.

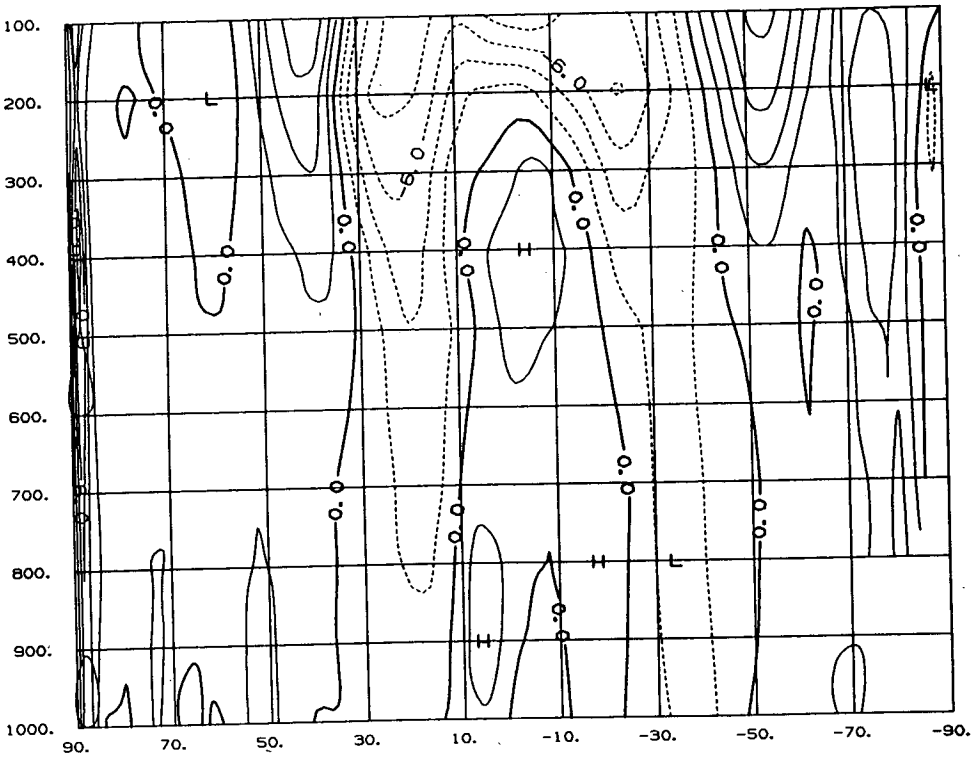

FIG. 4.3b. The DJFM mean of the zonal mean zonal wind error. The contour interval is 2 m s^{-1}. Dashed contours are negative.

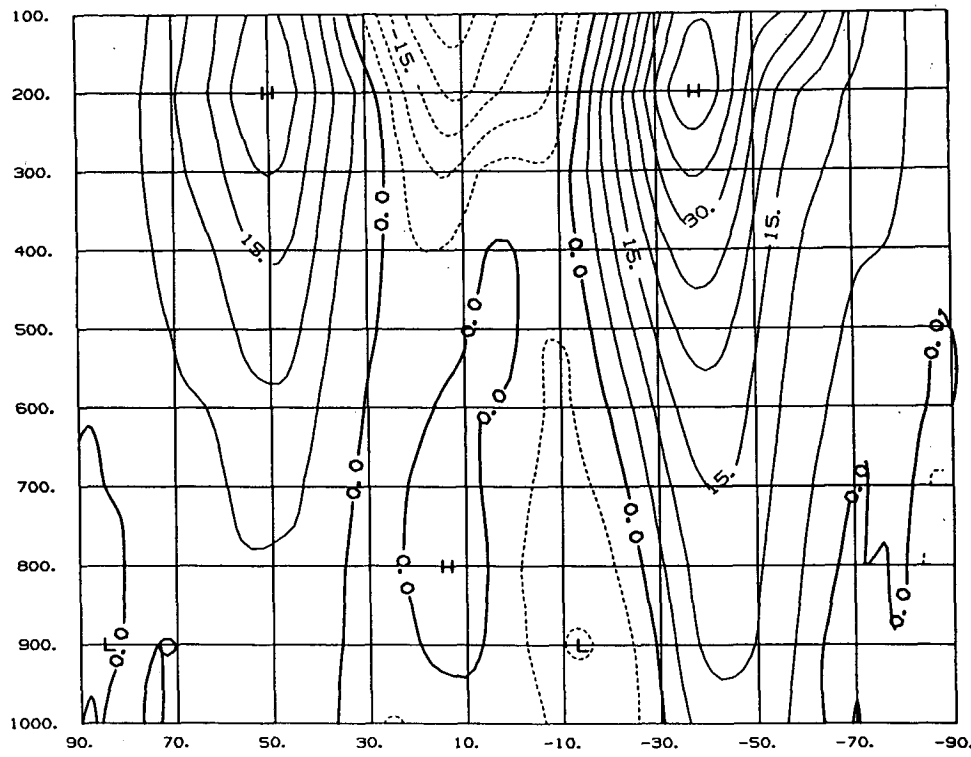

FIG. 4.4a. The MJJA mean of the simulated zonal mean zonal wind. The contour interval is 5 m s^{-1}. Dashed contours are negative.

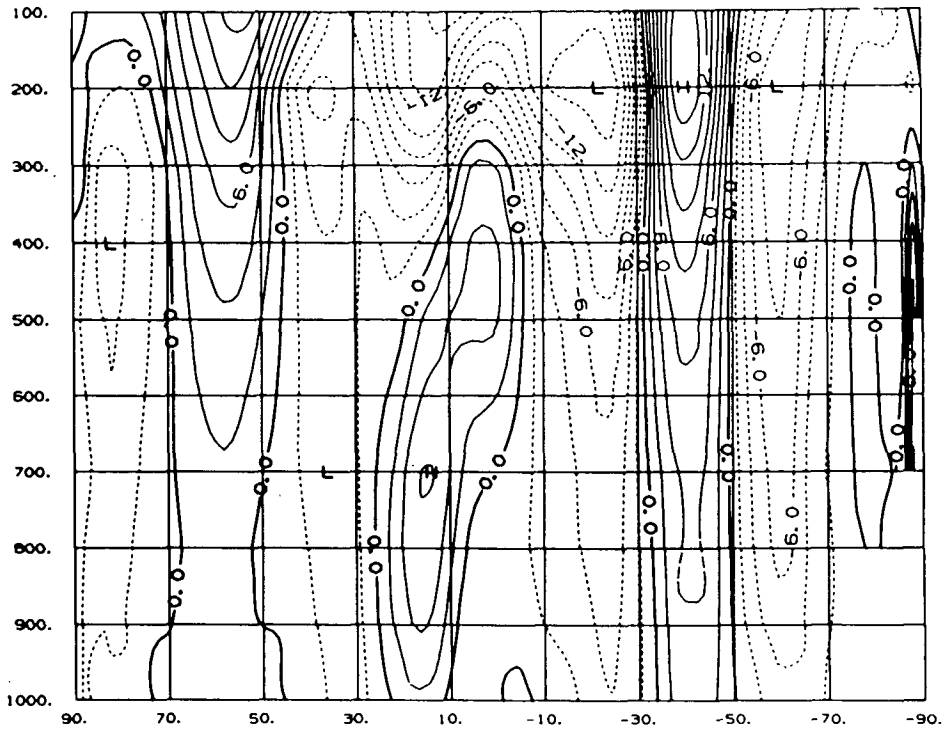

FIG. 4.4b. The MJJA mean of the zonal mean zonal wind error. The contour interval is 2 m s^{-1}. Dashed contours are negative.

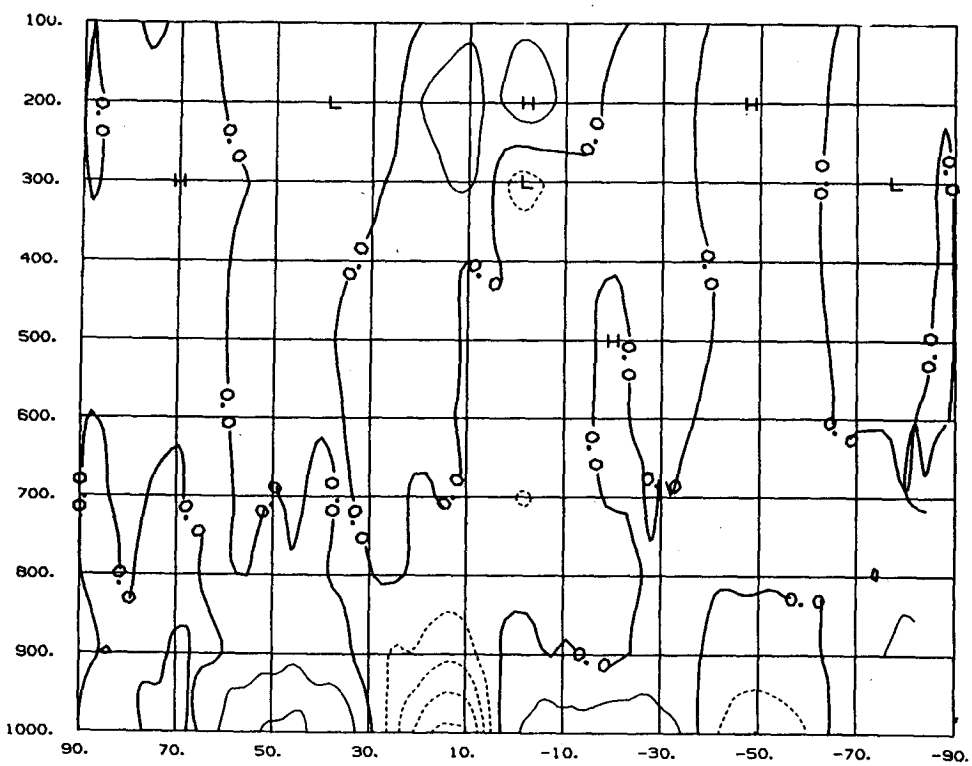

FIG. 4.5a. The DJFM mean of the simulated zonal mean meridional wind. The contour interval is 1 m s^{-1}. Dashed contours are negative.

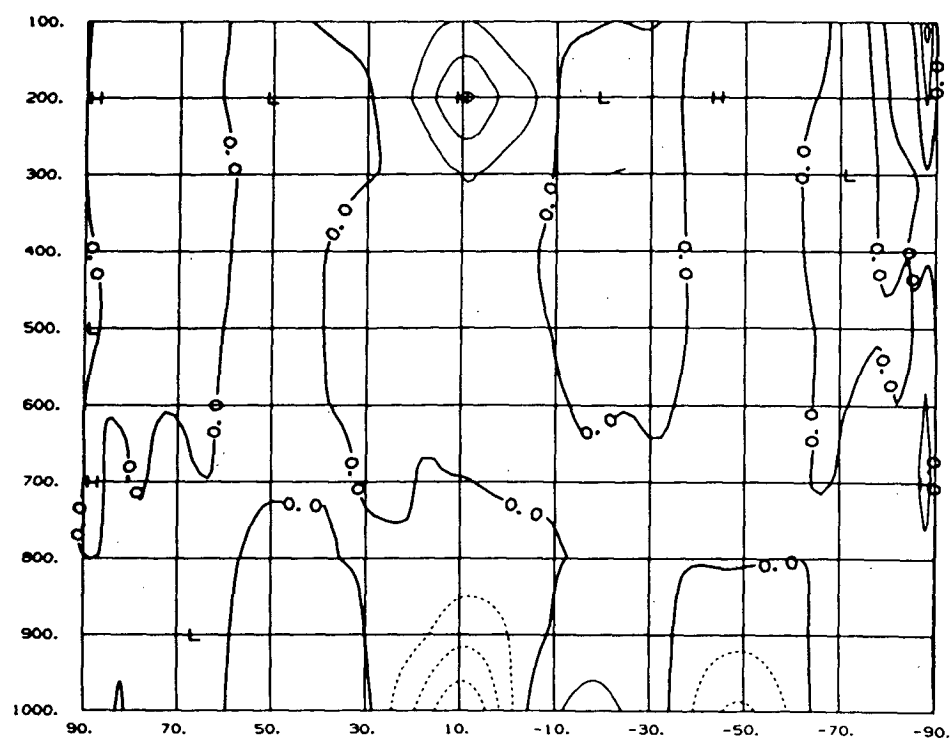

FIG. 4.5b. As in 4.5a except for observed zonal mean meridional wind.

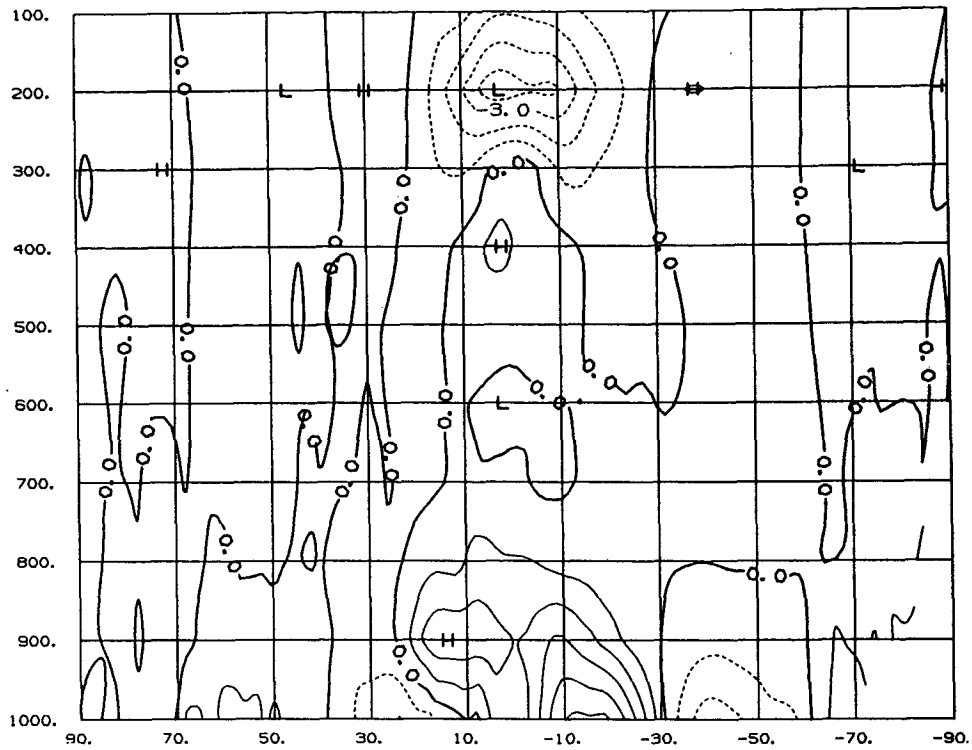

FIG. 4.6a. The MJJA mean of the simulated zonal mean meridional wind. The contour interval is 1 m s^{-1}. Dashed contours are negative.

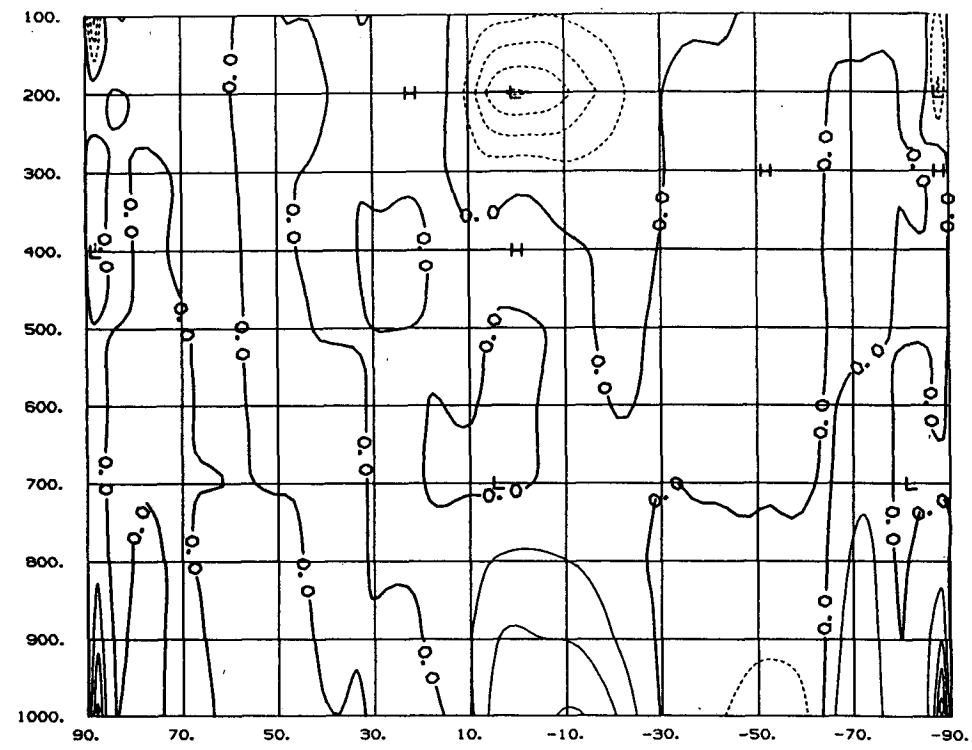

FIG. 4.6b. As in 4.6a except for observed zonal mean meridional wind.

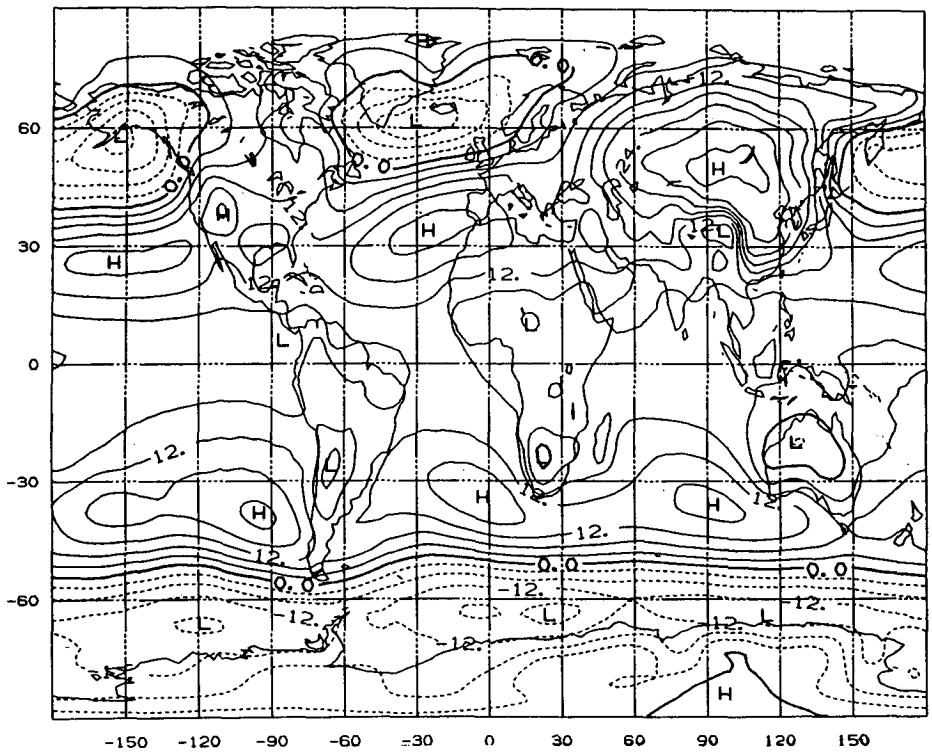

FIG. 4.7a. The DJFM mean of the simulated sea level pressure. The projection is cylindrical equidistant with the prime meridian in the center. The contour interval is 4 mb. Dashed contours are negative.

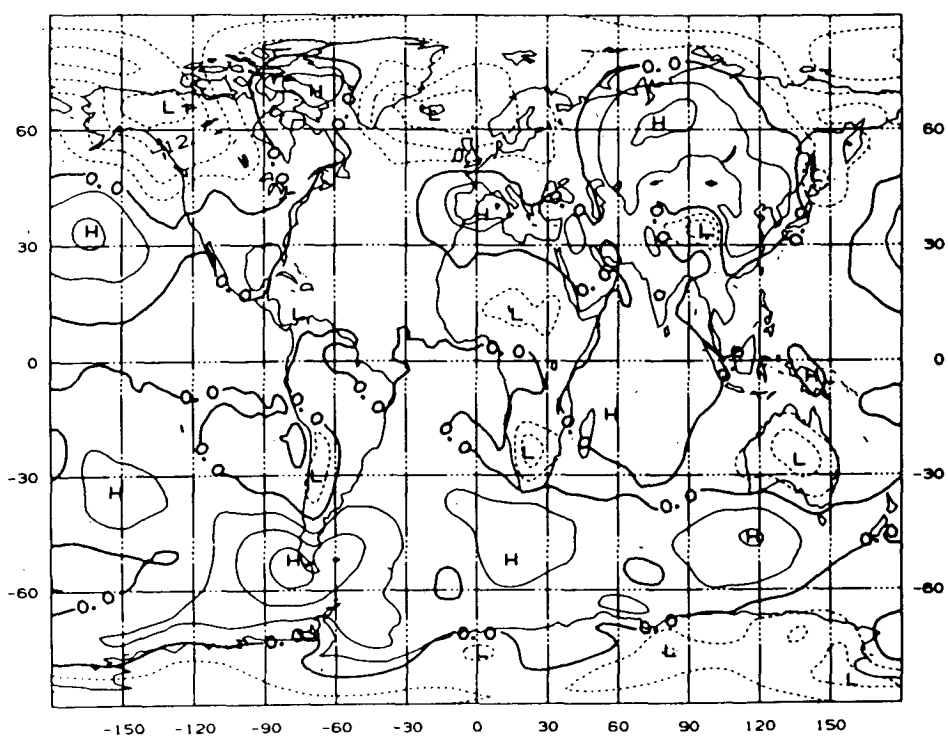

FIG. 4.7b. The DJFM mean of the sea level pressure error. The contour interval is 4 mb and the global mean bias of −3.9 mb has been subtracted. Dashed contours are negative.

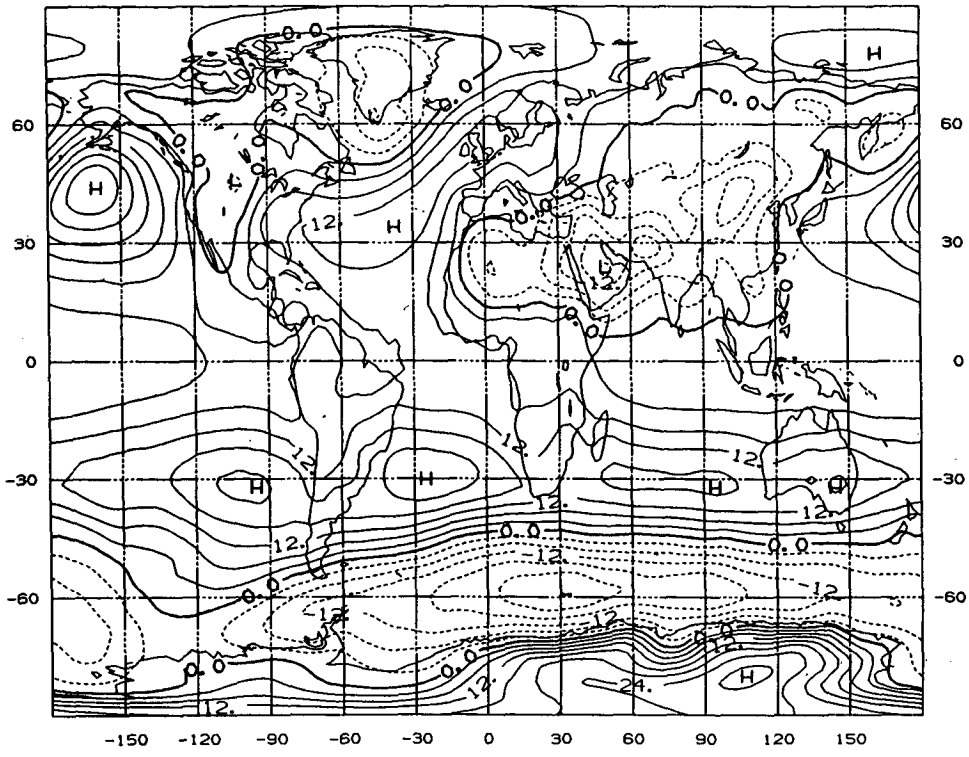

FIG. 4.8a. The MJJA mean of the simulated sea level pressure. The contour interval is 4 mb. Dashed contours are negative.

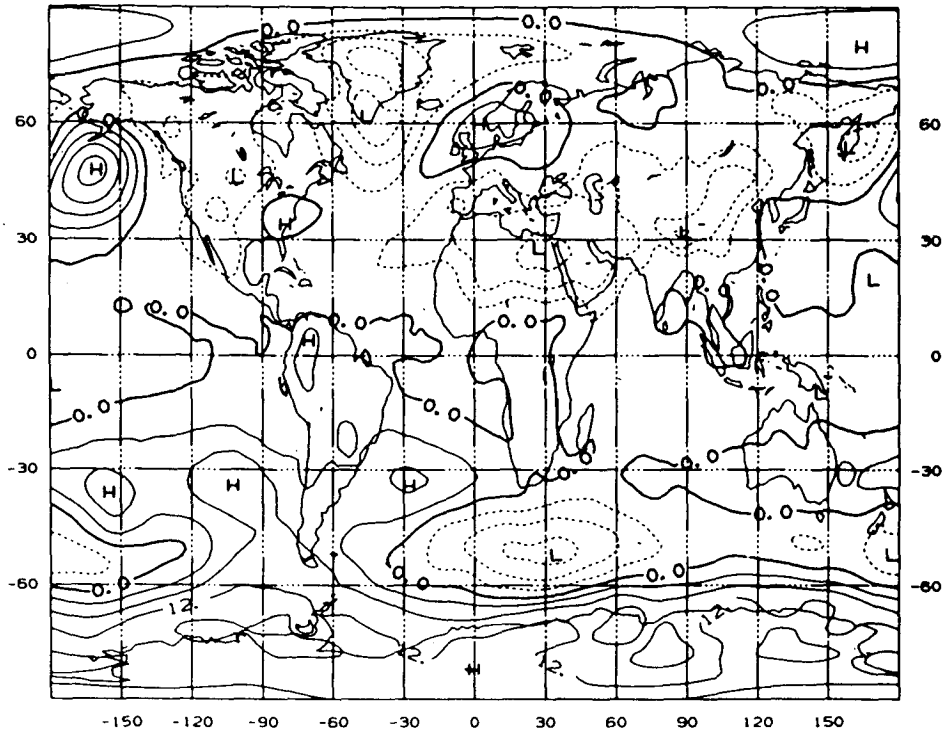

FIG. 4.8b. The MJJA mean of the sea level pressure error. The contour interval is 4 mb and the global mean bias of −4.0 mb has been subtracted. Dashed contours are negative.

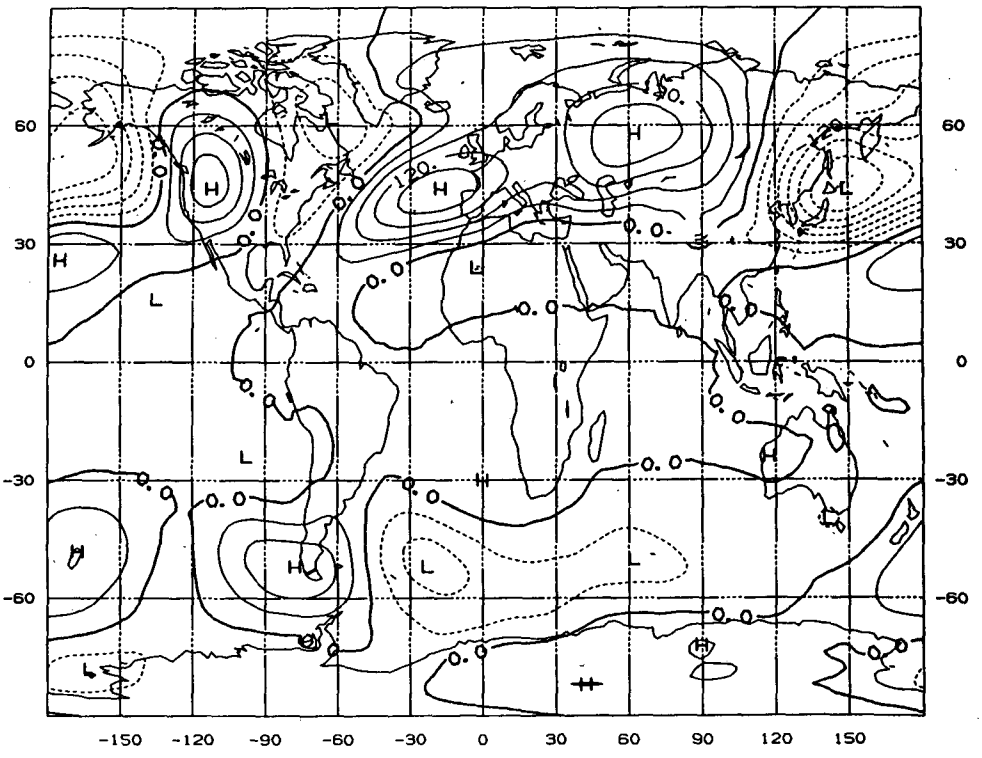

FIG. 4.9a. The DJFM mean of the simulated 500 mb eddy geopotential height. The contour interval is 40 m. Dashed contours are negative.

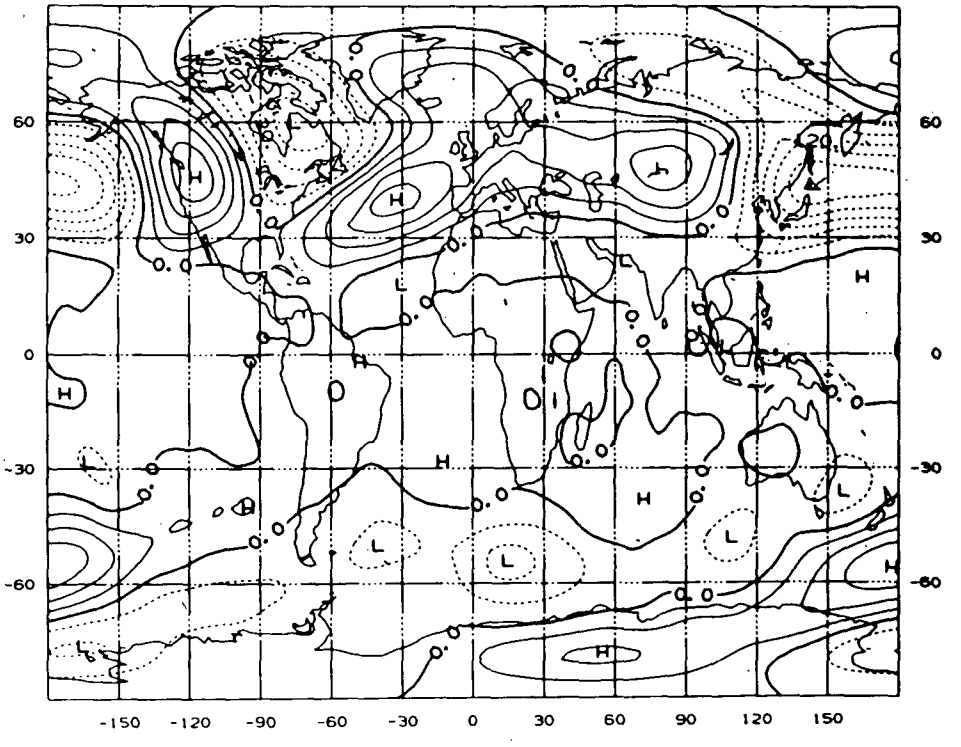

FIG. 4.9b. As in 4.9a except for observed 500 mb eddy geopotential height.

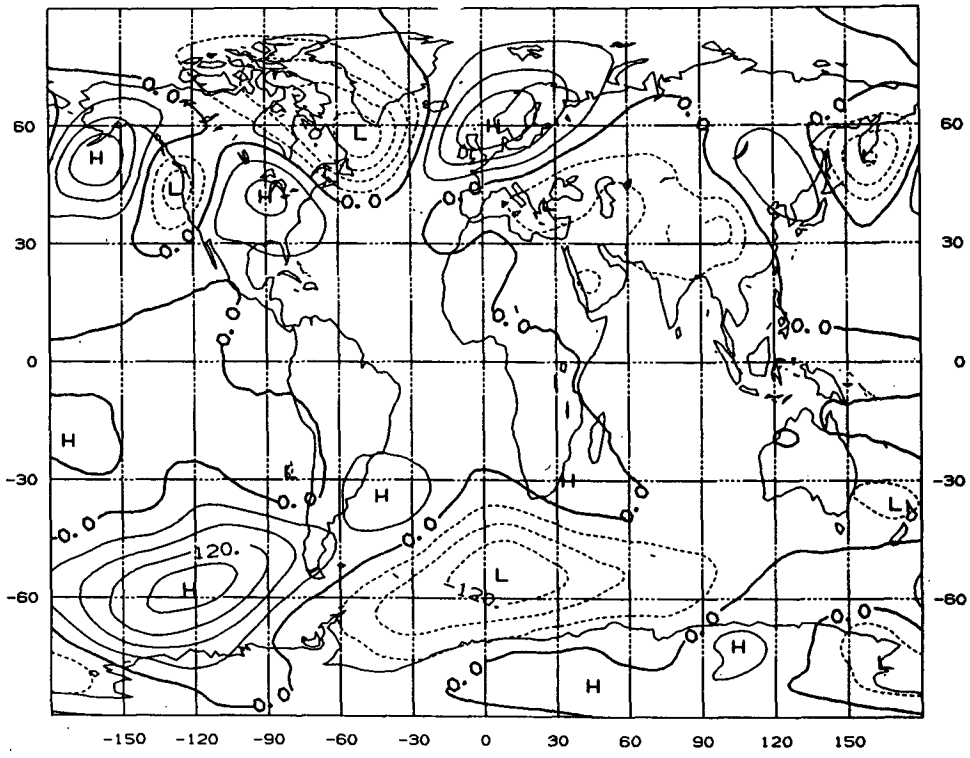

FIG. 4.10a. The MJJA mean of the simulated 500 mb eddy geopotential height. The contour interval is 40 m. Dashed contours are negative.

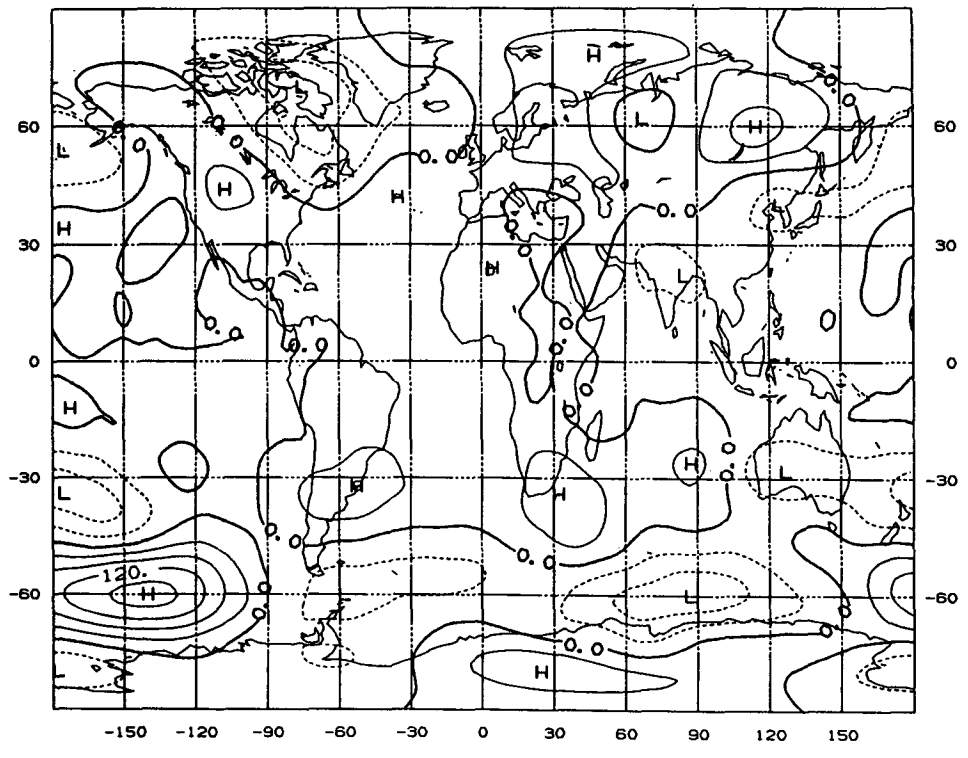

FIG. 4.10b. As in 4.10a except for observed 500 mb eddy geopotential height.

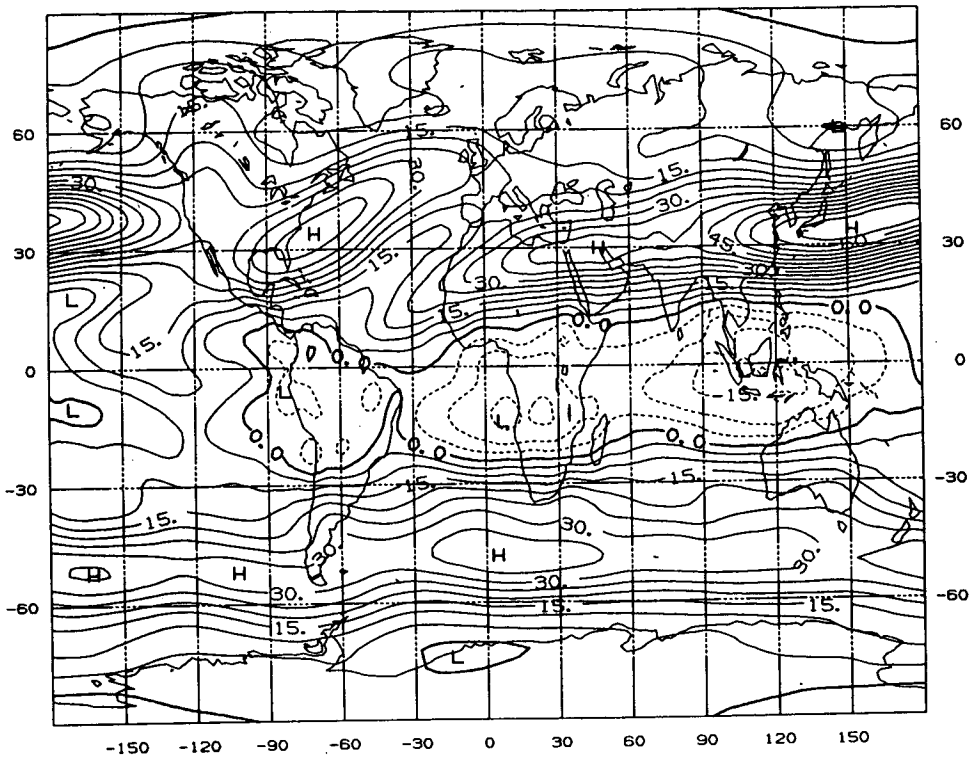

FIG. 4.11a. The DJFM mean of the simulated 200 mb zonal wind. The contour interval is 5 m s^{-1}. Dashed contours are negative.

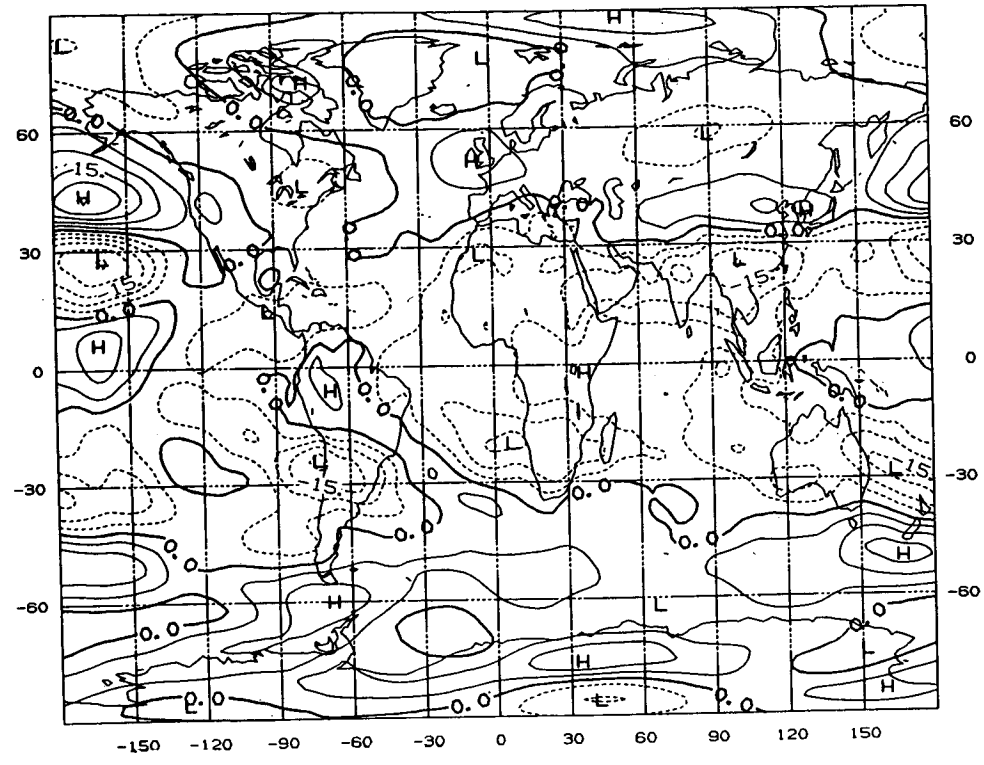

FIG. 4.11b. As in 4.11a except for 200 mb zonal wind error.

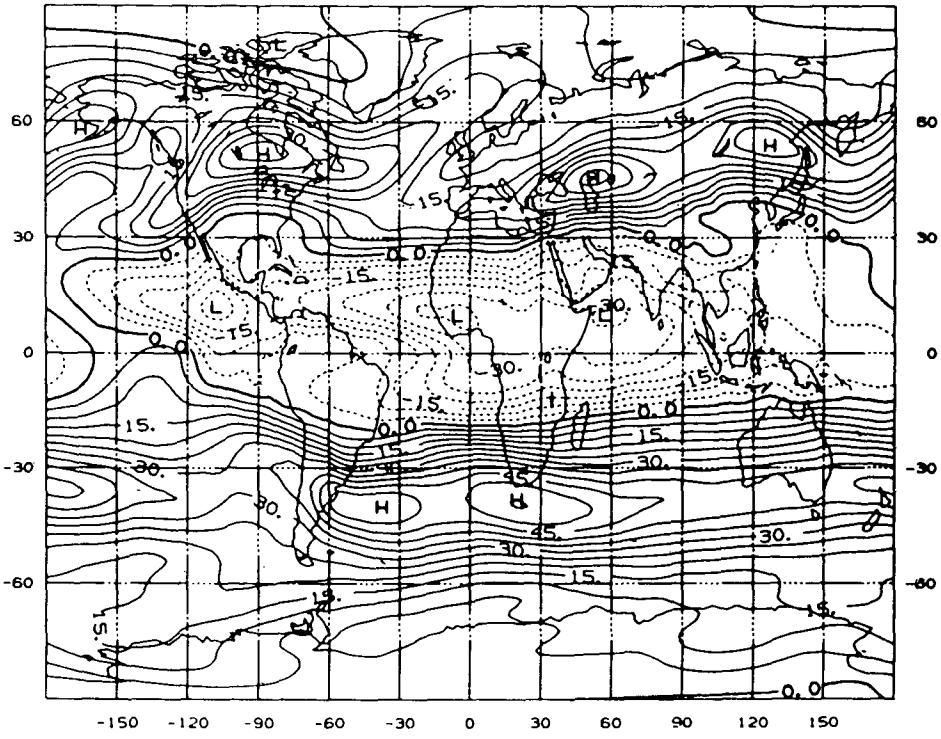

FIG. 4.12a. The MJJA mean of the simulated 200 mb zonal wind. The contour interval is 5 m s^{-1}. Dashed contours are negative.

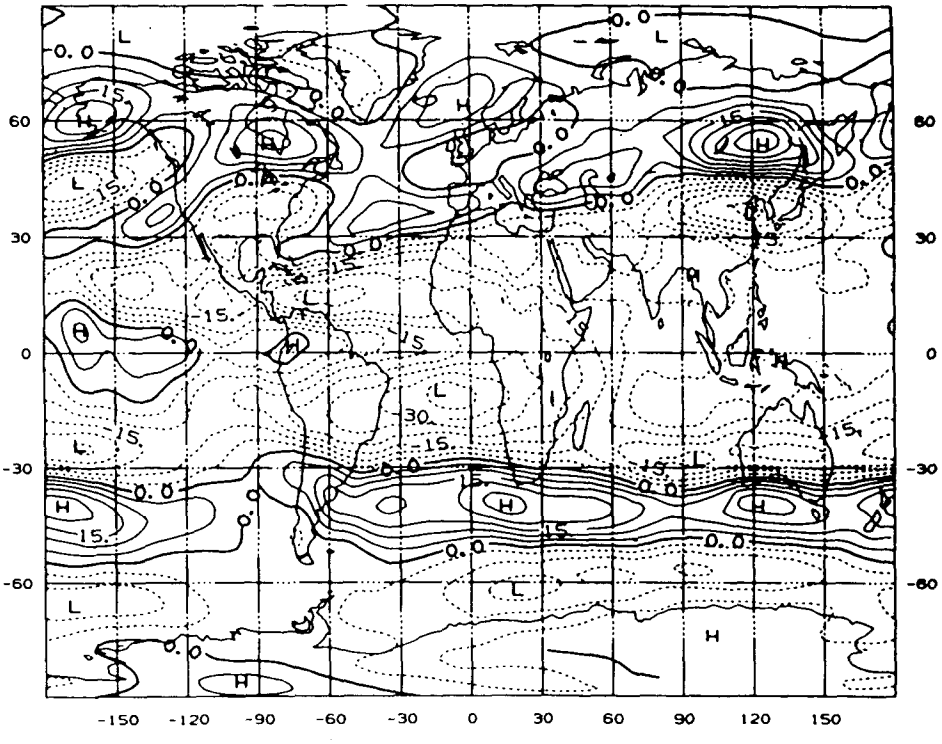

FIG. 4.12b. As in 4.12a except for 200 mb zonal wind error.

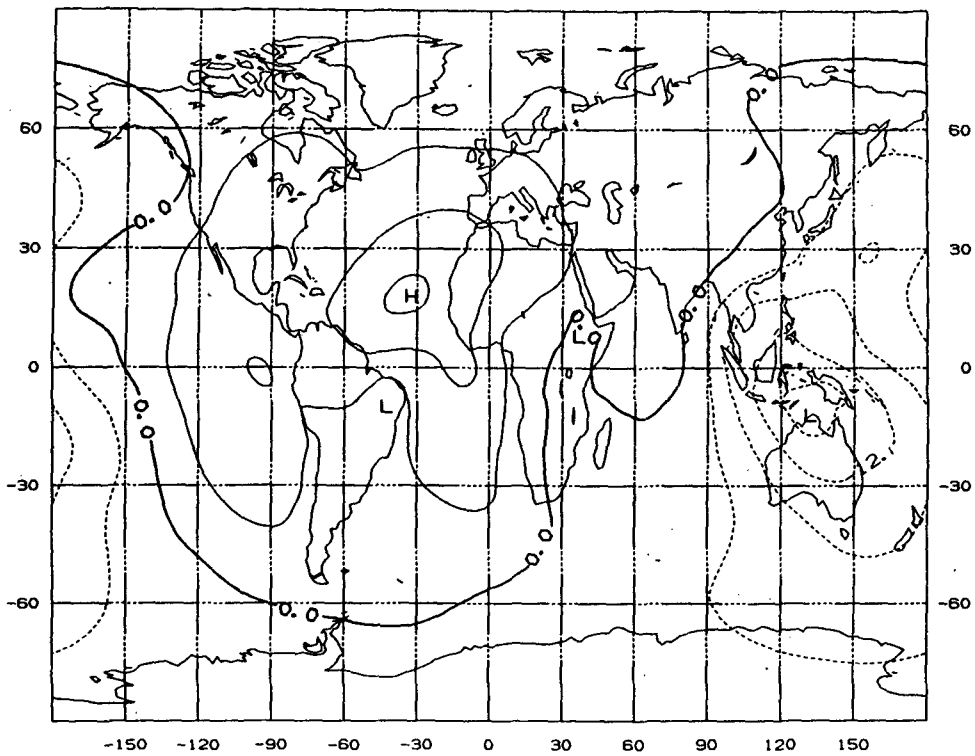

FIG. 4.13a. The DJFM mean of the simulated 200 mb velocity potential. The contour interval is 4×10^6 m^2 s^{-1}. Dashed contours are negative.

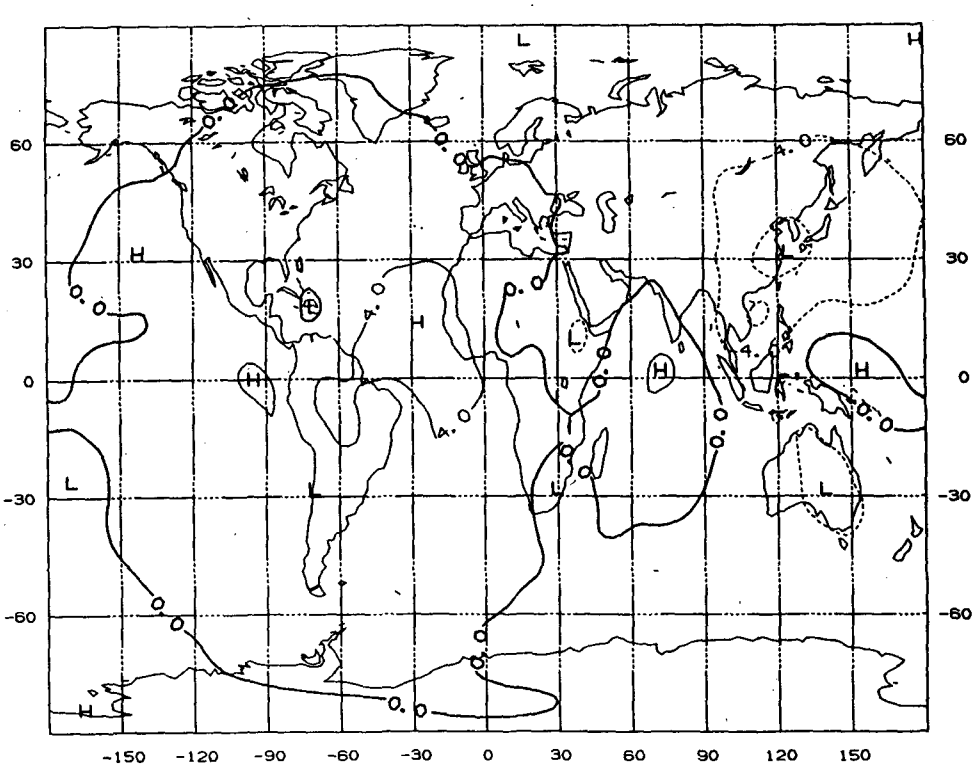

FIG. 4.13b. As in 4.13a except for 200 mb velocity potential error.

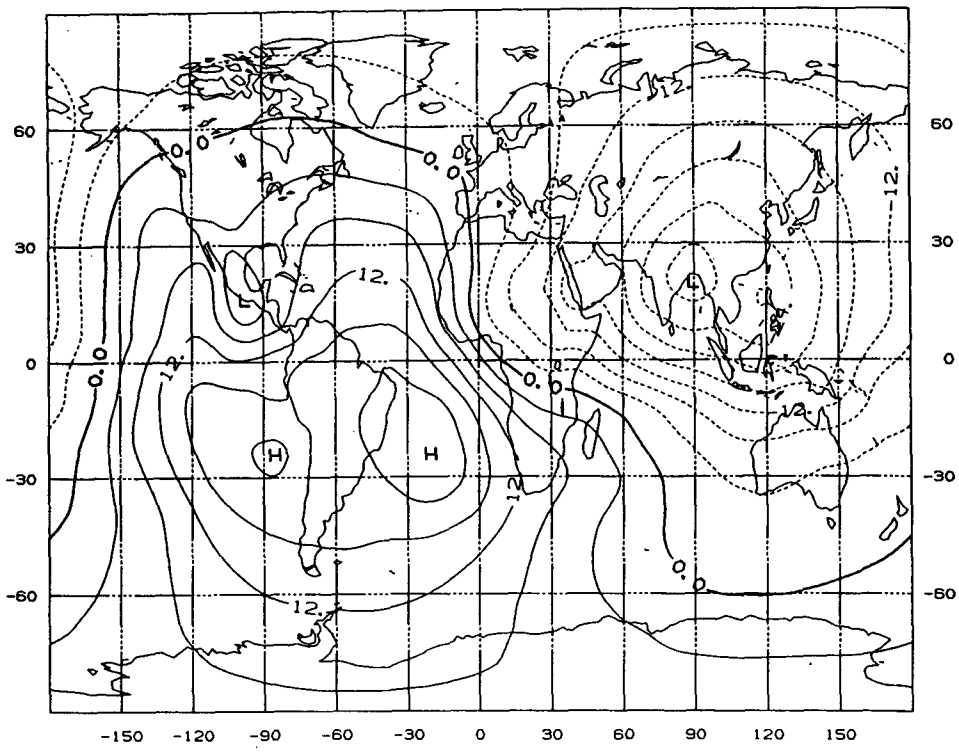

FIG. 4.14a. The MJJA mean of the simulated 200 mb velocity potential. The contour interval is 4×10^6 m^2 s^{-1}. Dashed contours are negative.

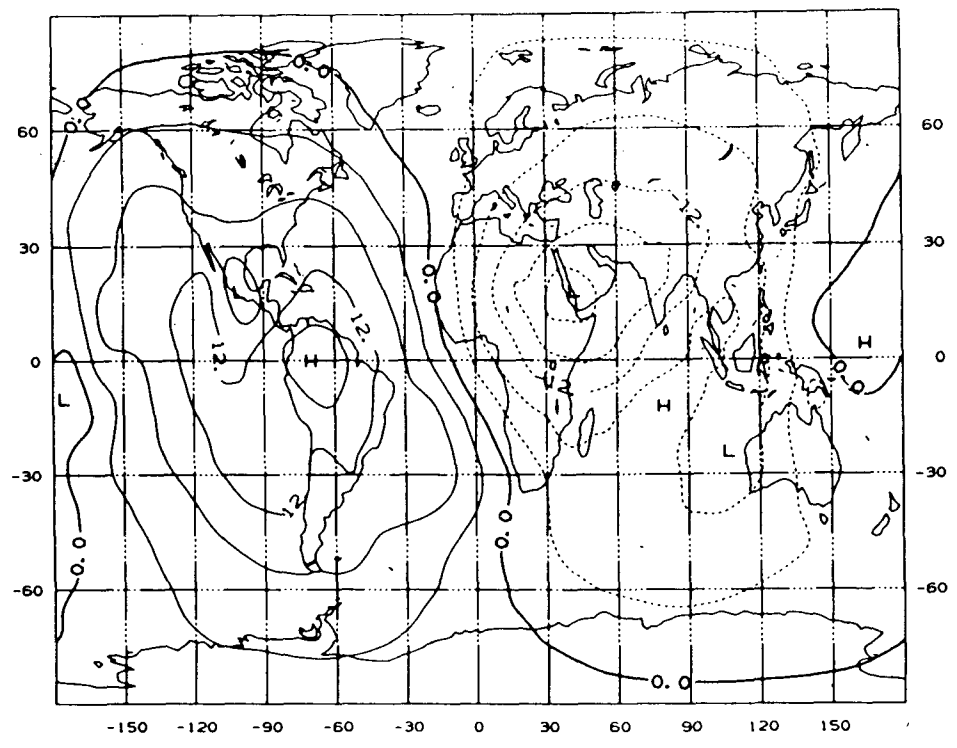

FIG. 4.14b. As in 4.14a except for 200 mb velocity potential error.

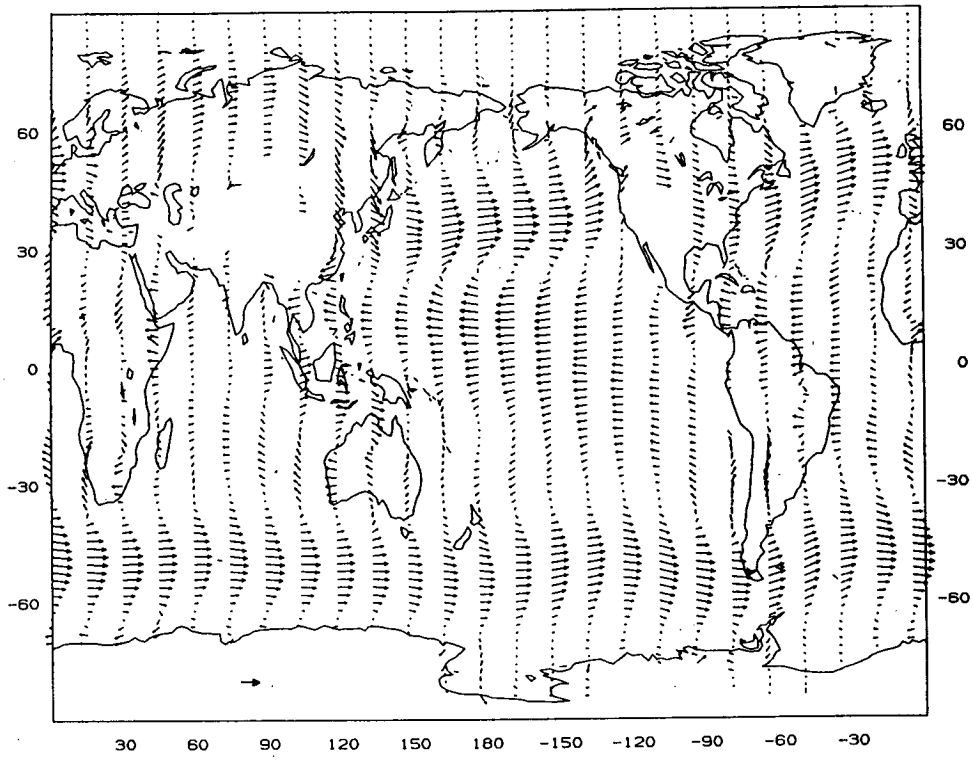

FIG. 4.15a. The DJFM mean of the simulated 850 mb vector velocity. The scaling vector is 10 m s^{-1}.

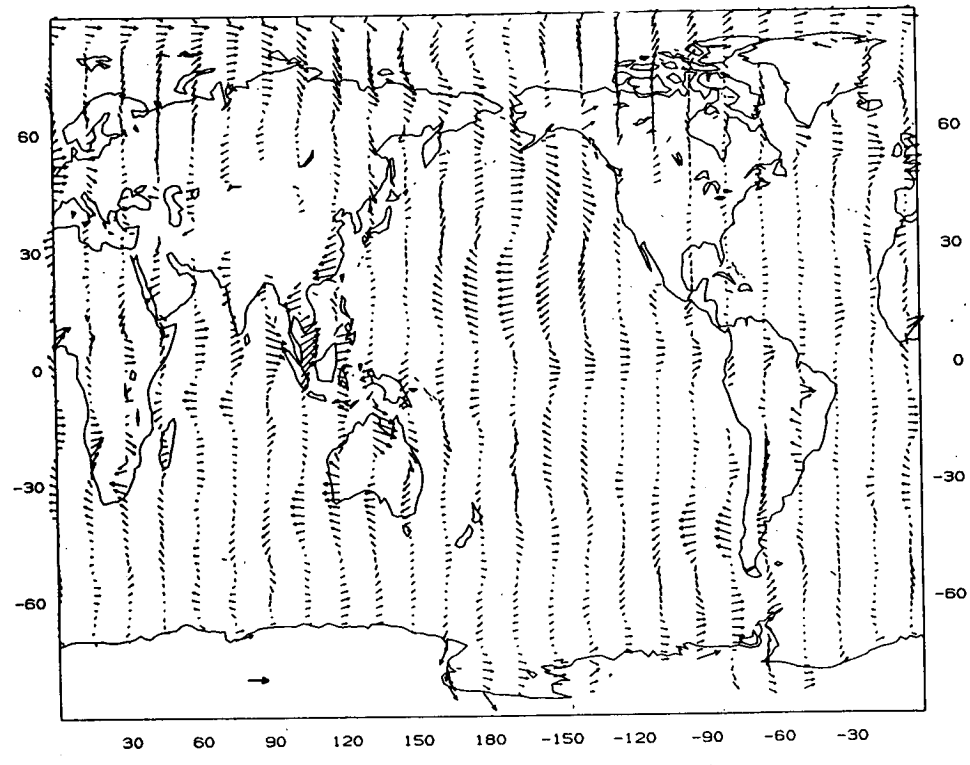

FIG. 4.15b. As in 4.15a except for 850 mb vector velocity error.

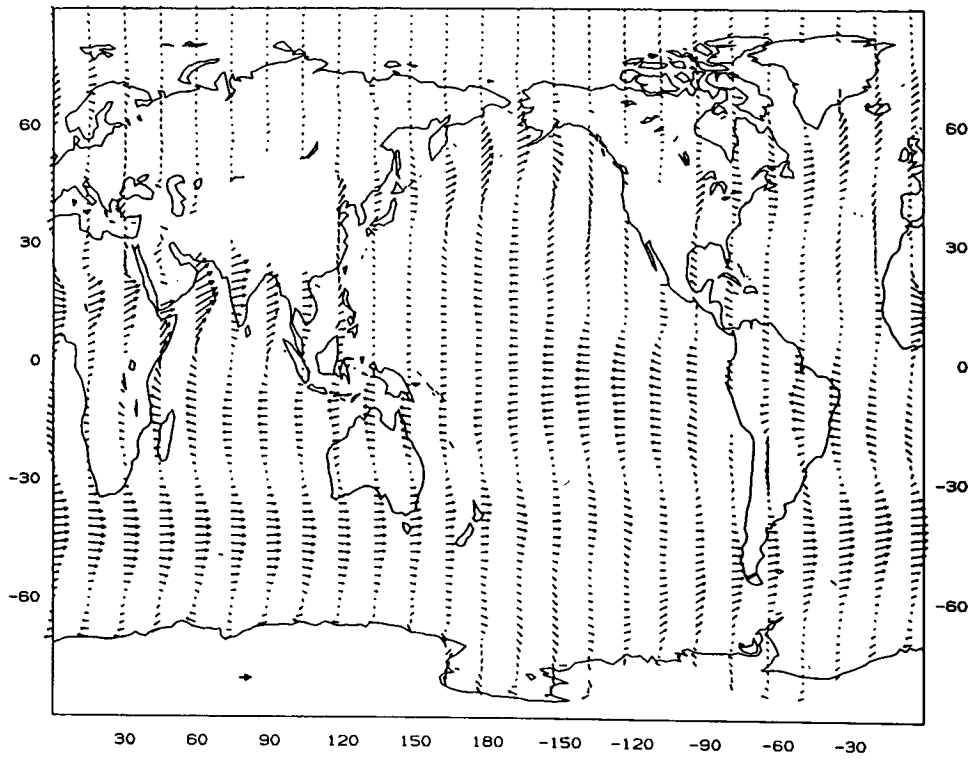

FIG. 4.16a. The MJJA mean of the simulated 850 mb vector velocity. The scaling vector is 10 m s^{-1}.

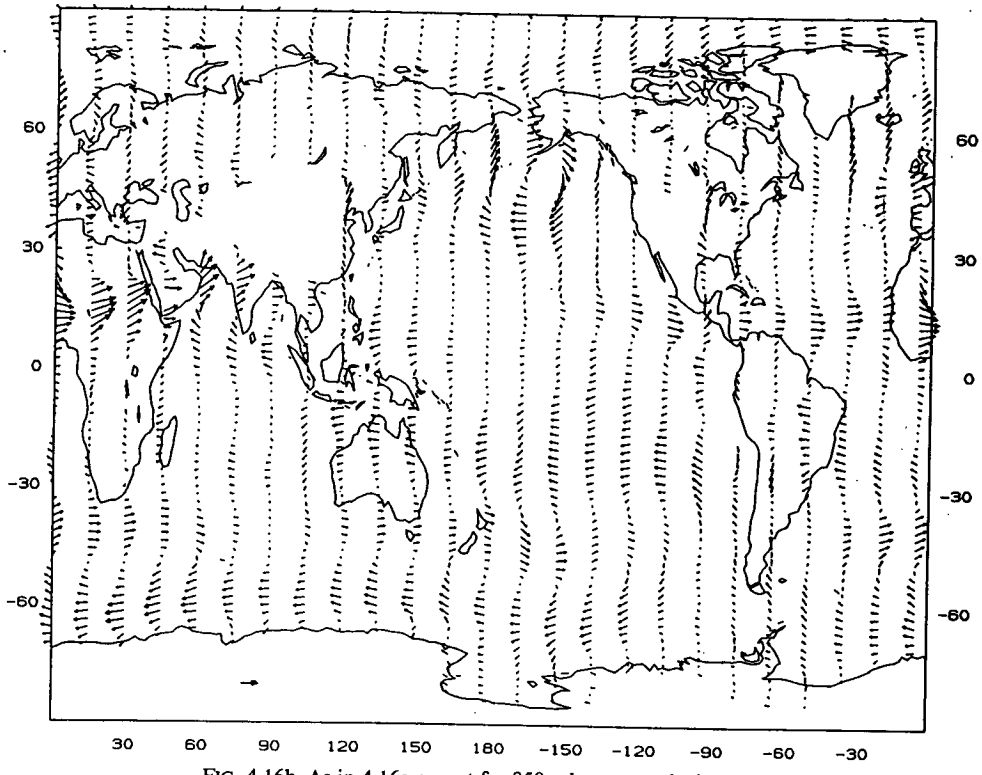

FIG. 4.16b. As in 4.16a except for 850 mb vector velocity error.

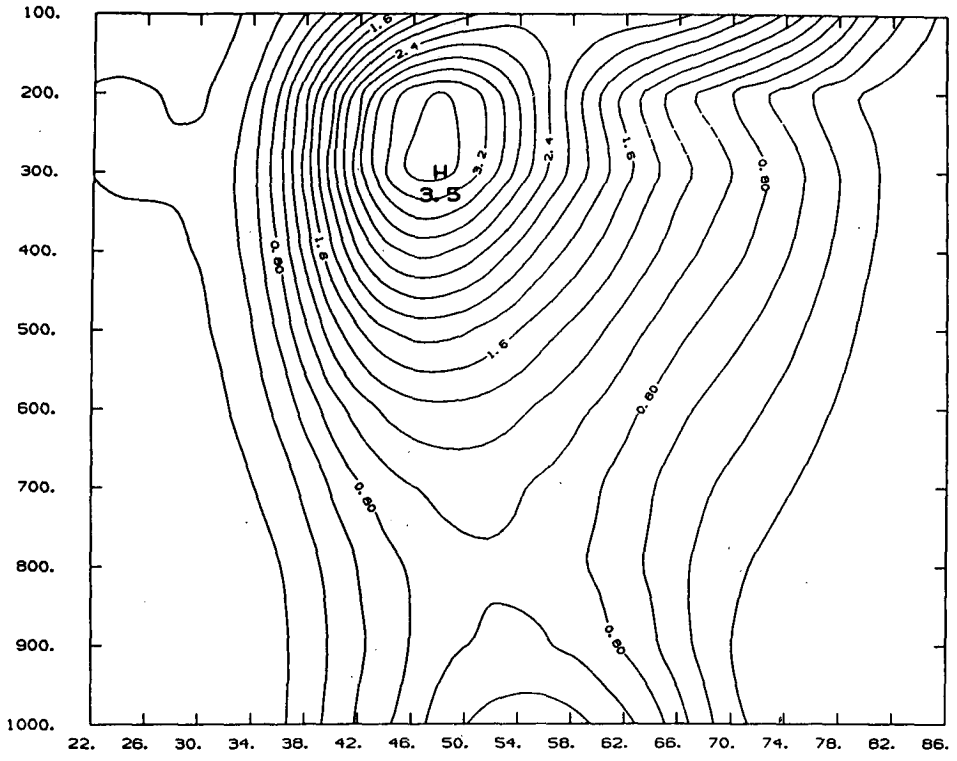

FIG. 5.1a. Simulated zonal mean of the geopotential height variance for the DJFM mean. The contour interval is 2×10^3 m^2.

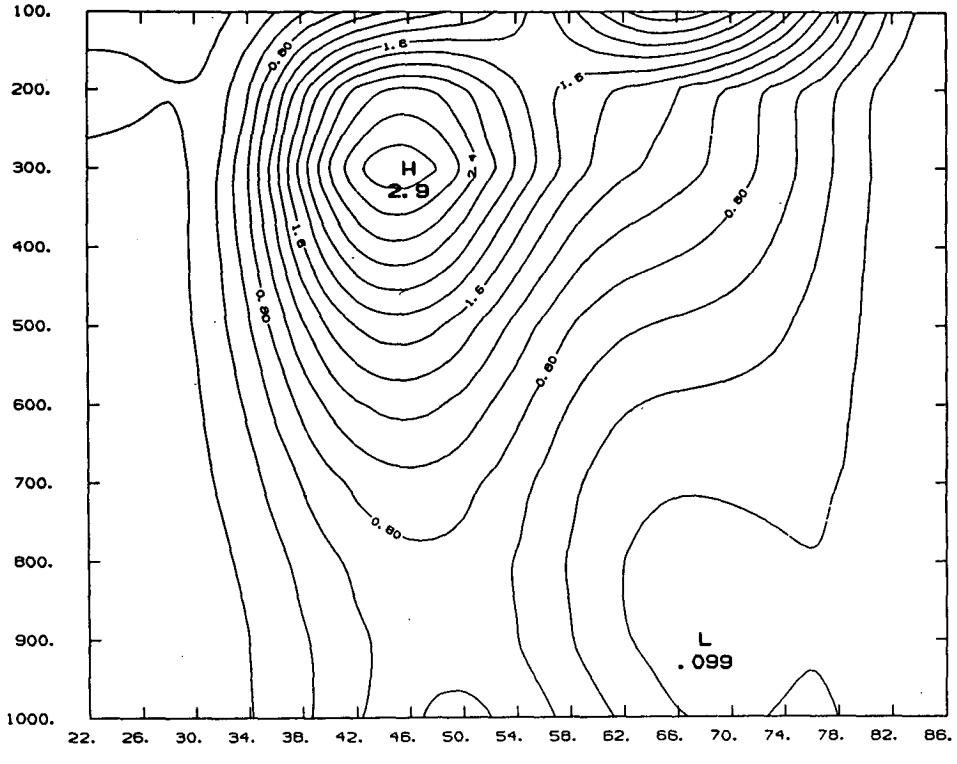

FIG. 5.1b. Observed zonal mean of the geopotential height variance for the DJFM mean. The contour interval is 2×10^3 m^2.

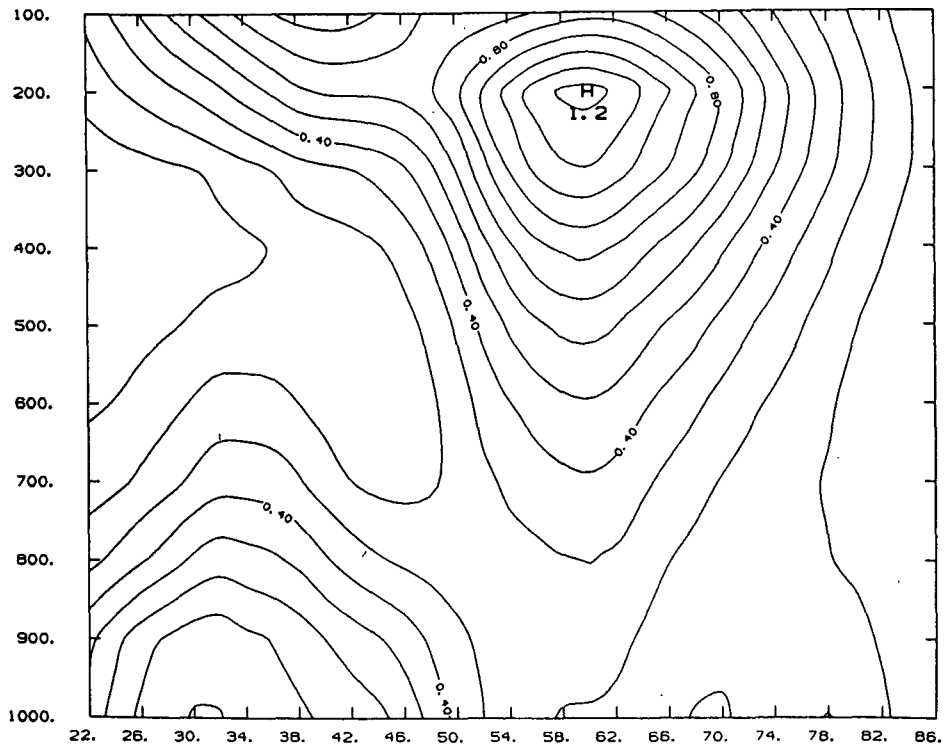

FIG. 5.2a. Simulated zonal mean of the geopotential height variance for the MJJA mean. The contour interval is 1×10^3 m^2.

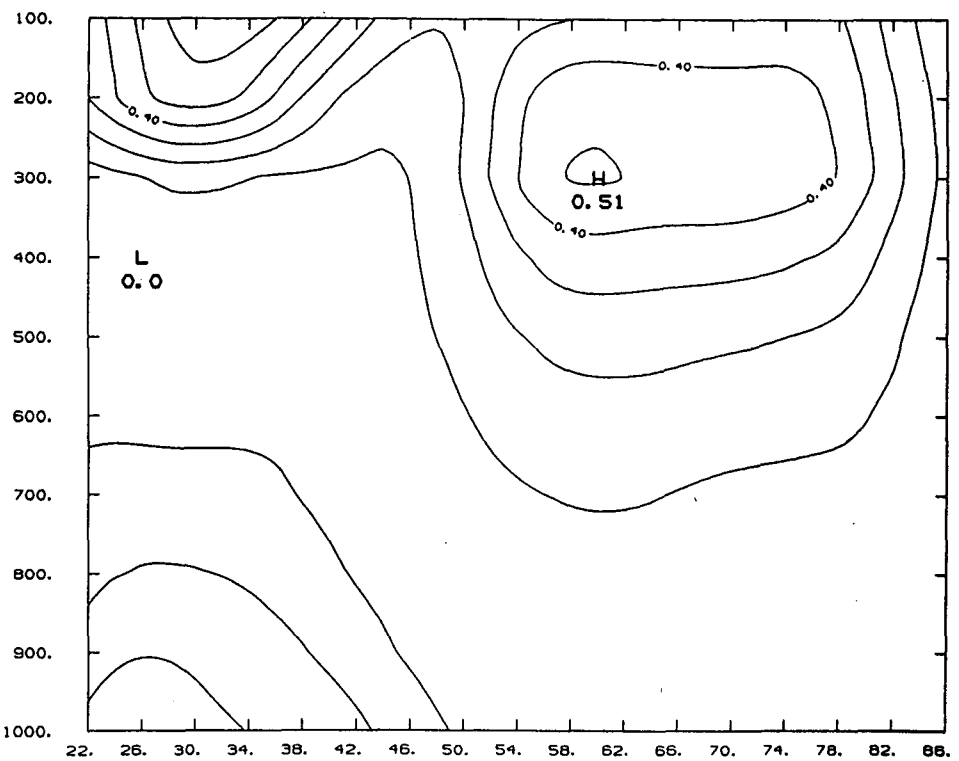

FIG. 5.2b. Observed znoal mean of the geopotential height variance for the MJJA mean. The contour interval is 1×10^3 m^2.

olation led to excessively low temperatures which caused the radiation calculation to fail. The model code was also modified to output several physical diagnostic quantities during the integration for the purpose of analyzing the model performance in greater detail.

The two simulations have been compared with the corresponding NMC analyses. These analyses are produced by the Global Data Assimilation System of NMC (Dey and Morone 1985). Although the analysis and forecast systems used by NMC change from time to time, the present investigation is an attempt to examine the dynamical properties of the model used for medium range forecasting during 1985–86. The data assimilation system at that time did not include the same model; however, the differences in the analyses are expected to be far less than the differences between the analyses and the model simulation.

3. Boundary conditions and fixed fields

As mentioned in section 2, the model is integrated with seasonally varying boundary conditions which are different from those used operationally by NMC. The boundary conditions were taken from a variety of sources judged to be among the most reliable climatologies rather than from daily operational analyses. In all cases, the monthly mean datasets were linearly interpolated to daily values to give a smooth seasonal variation.

The sea surface temperature (SST) used was a hybrid climatology computed by taking the Climate Analysis Center climatology (Reynolds 1982) in latitudes equatorward of 75 deg latitude and by using the Alexander and Mobley (1976) climatology poleward of that latitude. In addition, SST was modified under sea ice determined from a sea ice climatology (British Meteorological Office 1977) to be consistent with the GCM sea ice condition.

Soil moisture was prescribed from the monthly mean climatology prepared by Wilmott (1985) by resetting the soil moisture to the daily interpolated climatological value at the beginning of each model day. The surface albedo was prescribed as in Shukla et al. (1981), i.e., a modified version of the data described by Posey and Clapp (1964). A background snow cover field was computed based on this surface albedo dataset, but the

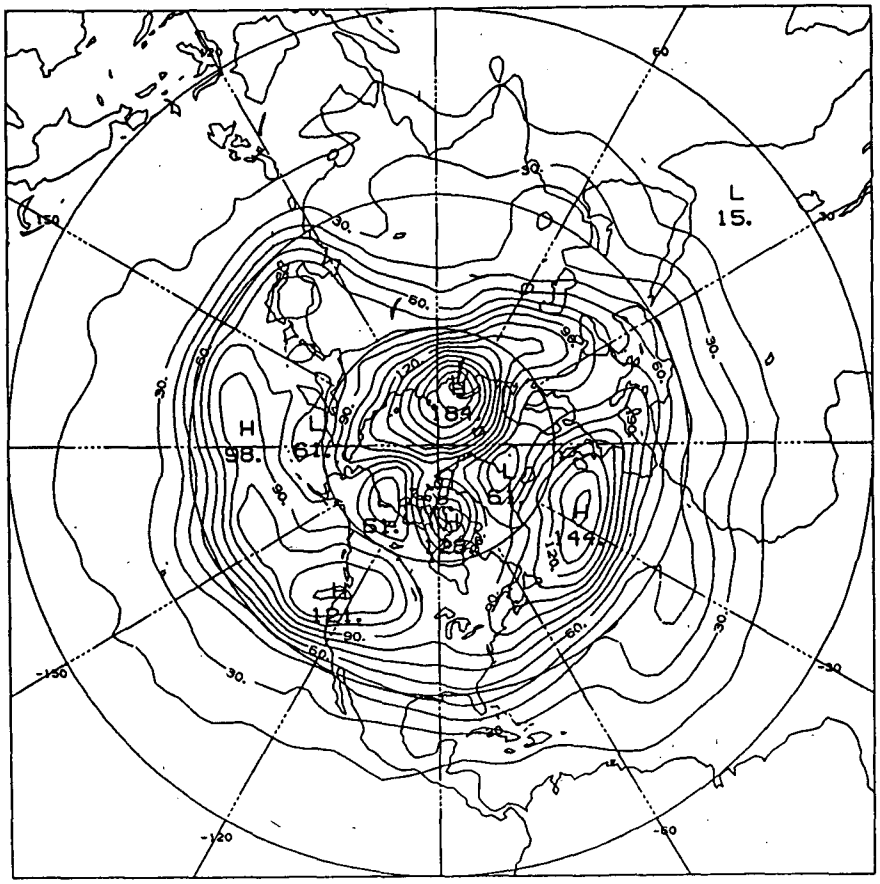

FIG. 5.3a. Simulated root-mean-square (RMS) deviation of 500 mb geopotential height from the DJFM mean after a parabolic fit to represent the seasonal cycle has been removed. The projection is polar stereographic. The contour interval is 10 m.

GCM was permitted to predict snowfall and accumulate it according to its prognostic snow equation over land. The cloudiness and ozone mixing ratio were also specified in the radiative transfer calculation; both were zonally symmetric, seasonal datasets used in the operational model.

The GCM physical parameterizations were computed on the Gaussian grid used to compute the nonlinear products in the hydrodynamics equations. Topographic heights and land–sea distributions were computed according to the "silhouette orography" algorithm of Mesinger (personal communication) as used in the operational model. The surface roughness length and deep ground temperature were also taken from the operational model datasets. Surface temperature at land grid points was initialized by means of an iterative technique assuming zero tendency in the surface temperature equation (a heat balance condition) as described by Miyakoda and Sirutis (1977).

4. Simulation of the time mean circulation

The model generated circulation is compared to the analyzed DJFM and MJJA means and also the long-period climatologies for the verifying periods. In each of the figures in this section, two panels are displayed. The first panel is the seasonal mean from the simulation; the second panel is either the seasonal mean from the verifying period of the NMC analyses, or the difference between the simulated seasonal mean and the analyzed seasonal mean. The NMC analyses are referred to as the observed state in the figure captions since the analysis represents the best estimate of the observed atmosphere, particularly with respect to this GCM.

In Fig. 4.1a, the zonally averaged temperature from the DJFM simulation is shown. We have only shown latitude–pressure cross sections up to the 100 mb level; the model has at least two sigma levels which are above the 100 mb level, but these are not shown. The vertical and horizontal temperature gradients are very similar to the analysis although the actual temperatures are smaller in the simulation by 4 to 8 K. The difference between the two (Fig. 4.1b) shows the error to be negative almost everywhere with a maximum centered near the tropopause in the winter hemisphere, reaching a value of over 10 K, and a second maximum in the summer lower stratosphere exceeding 12 K.

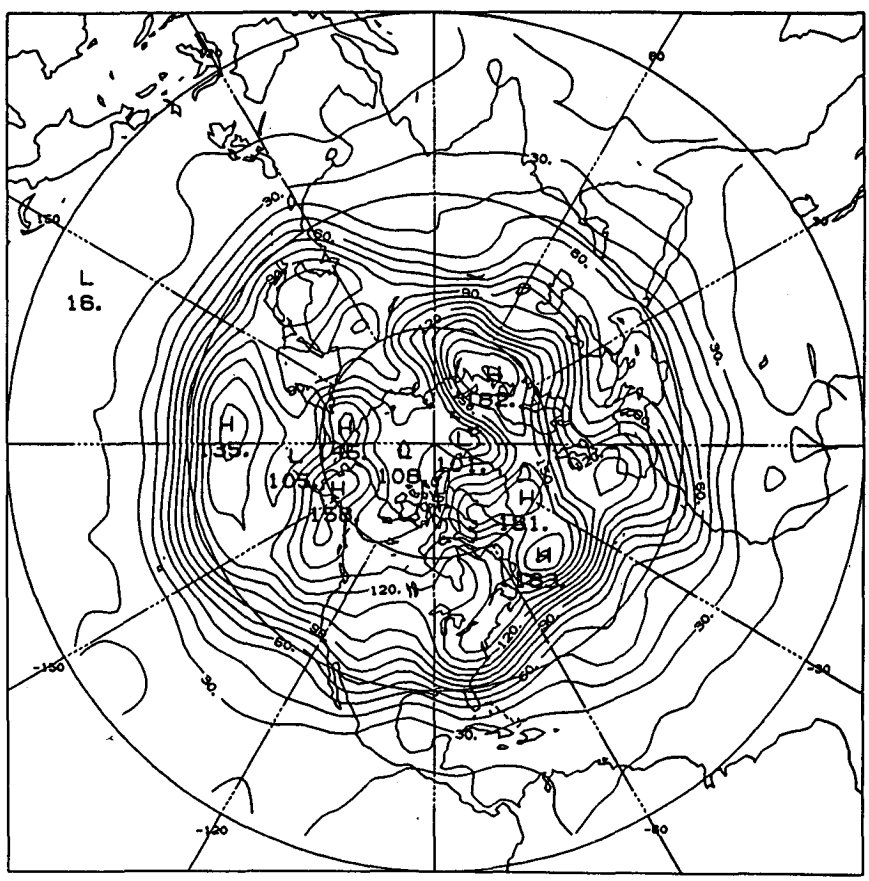

FIG. 5.3b. As in 5.3a except for observed RMS deviation.

The situation in the MJJA simulation (Figs. 4.2a and 4.2b as above) is much the same with the reversal of seasons taken into account. In particular, the summer lower stratosphere error maximum is of very nearly the same shape in both simulations and the tropical tropopause error is quite similar as well. The winter hemisphere error, however, does not reach a maximum at the tropopause but continues to increase with height into the winter lower stratosphere. Generally, the MJJA errors are larger than the DJFM errors by 1 to 5 K, particularly near the poles.

Consistent with the errors in the zonal mean temperature gradient implied in the preceding figures near the tropopause in the DJFM simulation, the zonal mean zonal wind has a subtropical jet which is displaced poleward of its analyzed position (see Fig. 4.3a). The magnitude of the wind at the jet core is nearly the same as its analyzed value in both winter and summer hemispheres. The simulation of this feature by the NMC model is far superior to that of, for example, the GLAS climate model (Shukla et al. 1981). The model error in Fig. 4.3b has a relatively strong easterly bias in the upper tropical troposphere and its surface tropical easterlies are weaker than observed. The MJJA zonal wind error (Fig. 4.4b) is an exaggerated version of the DJFM error. The tropical easterly bias above 300 mb is even stronger in MJJA, reaching a maximum in excess of 12 m s^{-1}. The latitudinal shifts of the subtropical jets from their analyzed positions is more marked in MJJA than in DJFM and the jet cores have winds nearly 5 m s^{-1} stronger than observed.

The seasonal means of the mean meridional circulation of the model (Figs. 4.5a and 4.6a) may be seen to be different from their analyzed values (Figs. 4.5b and 4.6b), with percentage errors as large as the percentages errors in the temperature distribution and zonal winds. In the DJFM simulation, features of the Hadley and Ferrel cells near the surface resemble the analyzed features, but the mean meridional circulation is weaker than analysis near the tropical tropopause. The MJJA simulation, in contrast to other features presented so far, has a more realistic Hadley cell than the DJFM simulation. The mean error of the MJJA mean meridional circulation (not shown) is less than 1.5 m s^{-1} nearly everywhere except near the surface at the North Pole and at 20°S. It may also be noted in Figs. 4.5 and 4.6 that the zonal mean confluence line near the surface in the tropics is 6 deg north of its

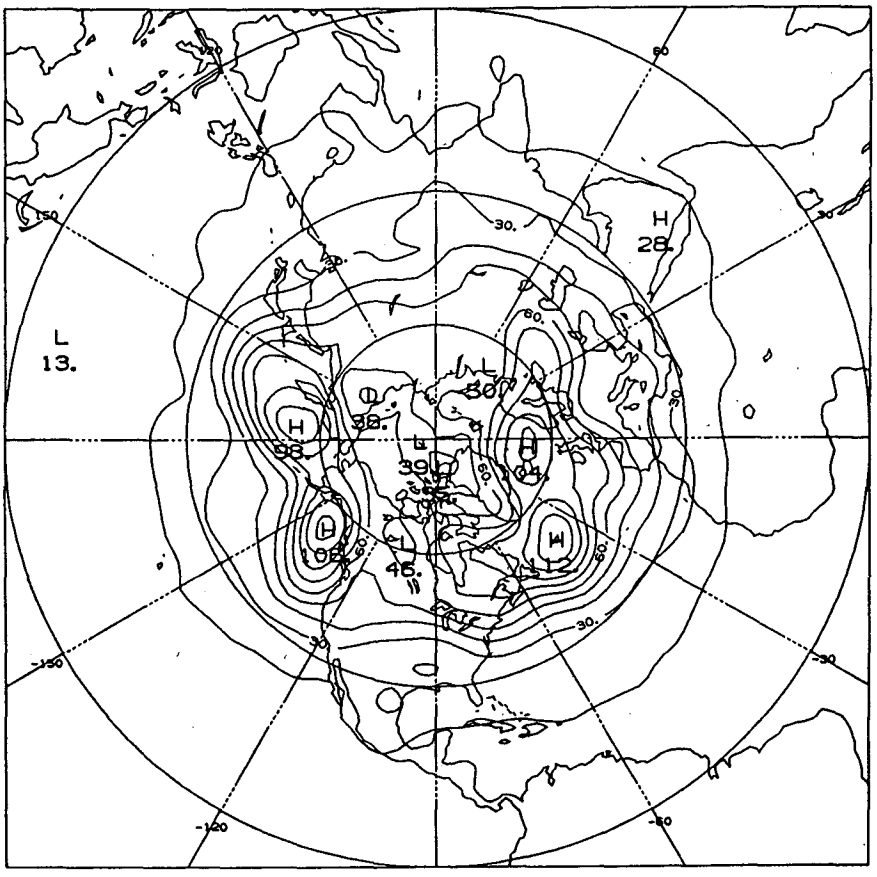

FIG. 5.4a. Simulated RMS deviation of 500 mb geopotential height from the MJJA mean after a parabolic fit to represent the seasonal cycle has been removed. The contour interval is 10 m.

observed position in DJFM and about 5 deg south of its observed position in MJJA.

Among the better features of both simulations are the sea level pressure means shown in Figs. 4.7a and 4.8a. It should be noted that the global mean surface pressure decreased linearly with time during both integrations at a rate of about 0.09 mb day^{-1}. This resulted in a global mean, seasonal mean sea level pressure bias of approximately −4 mb in both cases. This bias was subtracted from the error fields shown in Figs. 4.7b and 4.8b. In general, the observed winter midlatitude oceanic lows and continental highs, the subtropical oceanic highs, the summer subtropical highs over the oceans and continental lows, and the band of low pressure over the Southern Ocean are all well simulated. The model produces Aleutian and Icelandic lows which are more intense than observed in the DJFM simulation, and pressures are too low over Greenland and the East Asian monsoon region in MJJA. The mean errors have the same pattern and sign as the observed anomalies (not shown) so that the use of observed boundary conditions rather than climatological boundary conditions might have reduced the deficiencies in both simulations. The model also shifted some of the subtropical highs (notably the high off the west coast of Chile in DJFM and the high off the west coast of California in MJJA) poleward of their observed positions. Simulated pressure over North Africa is too low in both simulations.

The simulated and analyzed eddy 500 mb height distributions are shown in Figs. 4.9 and 4.10. In general, the simulated phases of the climatological ridges and troughs in the upper tropospheric winter hemisphere are in agreement with their analyzed values in midlatitudes, but the amplitudes of the waves are smaller than analysis. This is broadly true for simulations of both seasons. For example, Fig. 4.9a shows stationary ridges over the western half of North America, southwestern Europe and western Soviet Union. These three simulated ridges are similar to analyzed features, although the European ridge was analyzed to be centered more over the Atlantic Ocean than over the continent (Fig. 4.9b). The simulated stationary troughs over the eastern half of North America, Japan and most of the North Pacific are also as analyzed although the phase tilts are not altogether the same. In the summer hemisphere, however, the model simulated the stationary waves very poorly, particularly in DJFM.

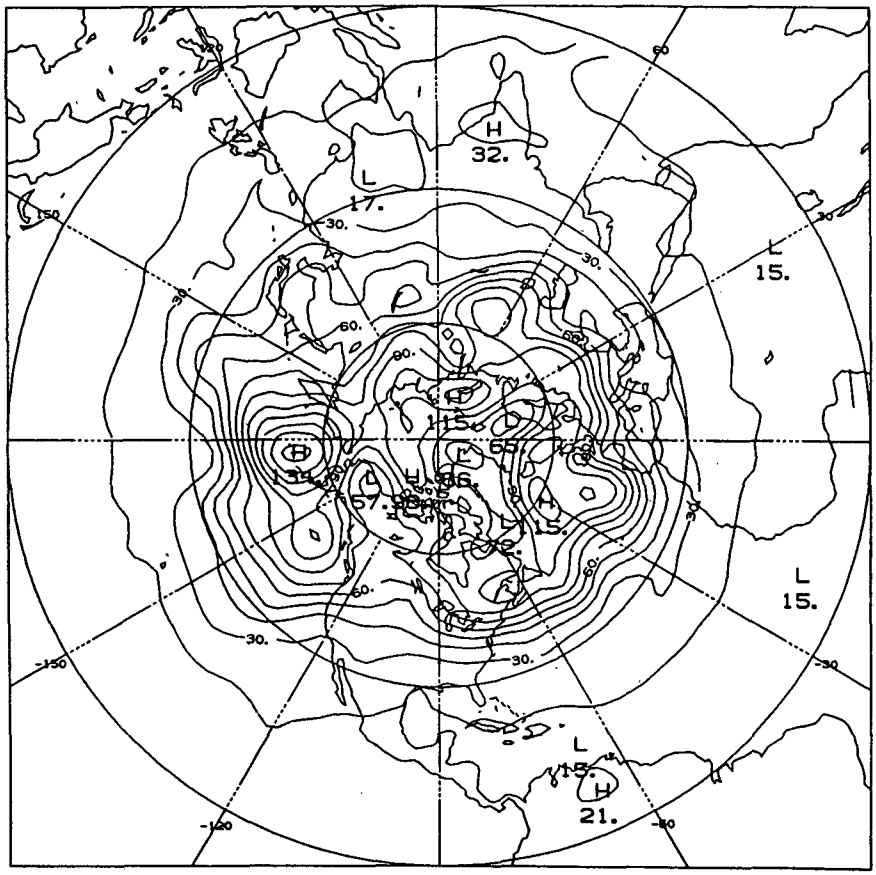

FIG. 5.4b. As in 5.4a except for observed RMS deviation.

The DJFM zonal wind at 200 mb, shown in Fig. 4.11, is reasonably well simulated. While GCMs typically form a zonal band of upper tropospheric zonal wind at 35°–40°N in the winter without the observed breaks over western North America and the eastern Atlantic Ocean, Fig. 4.11a shows these breaks to be simulated in this experiment. In fact, the zonal wind distribution north of 30°N in DJFM is very close to analysis everywhere except over the northeastern Pacific Ocean where the subtropical jet exit region is displaced 5 deg north of its analyzed position. This cannot be said for the MJJA simulation in which the zonal wind errors at 200 mb are quite large over most of the summer hemisphere (Fig. 4.12b). The strong easterly bias in the tropics is pronounced in MJJA, and the subtropical jet in the winter hemisphere is well poleward of its analyzed position.

The DJFM velocity potential at 200 mb, shown in Fig. 4.13a has a pronounced minimum over the Indonesian region which is in reasonable agreement with the analysis. A weak maximum over the north-tropical Atlantic is also simulated by the model except that it is too intense in the model. The observed maximum over northern Asia and the eastern Soviet Union is not simulated by the model giving rise to negative values over that region in the difference map (Fig. 4.13b). The simulated (Fig. 4.14a) velocity potential map at 200 mb for MJJA resembles the analyzed map (not shown); however, the analyzed minimum near southeast Asia is displaced westward by more than 40 deg of longitude in the simulation. The magnitude of the error (Fig. 4.14b) in the summer season velocity potential is comparable to the total field with displaced locations of maxima and minima. This may be a manifestation of the erroneous simulation of the precipitation field during the summer season which will be discussed in section 6.

Figures 4.15 and 4.16 show the horizontal velocity vectors at 850 mb for the DJFM and MJJA seasons, respectively. The general pattern of easterlies and westerlies is simulated reasonably well in both seasons. The locations of the simulated zero wind lines over the oceans are quite close to their analyzed locations. A complete reversal of the winds over the Arabian Sea and the adjoining areas from winter to summer in association with the onset of the Asiatic summer monsoon is captured by the model. There are discrepancies, however, in the magnitudes of the wind vectors. For

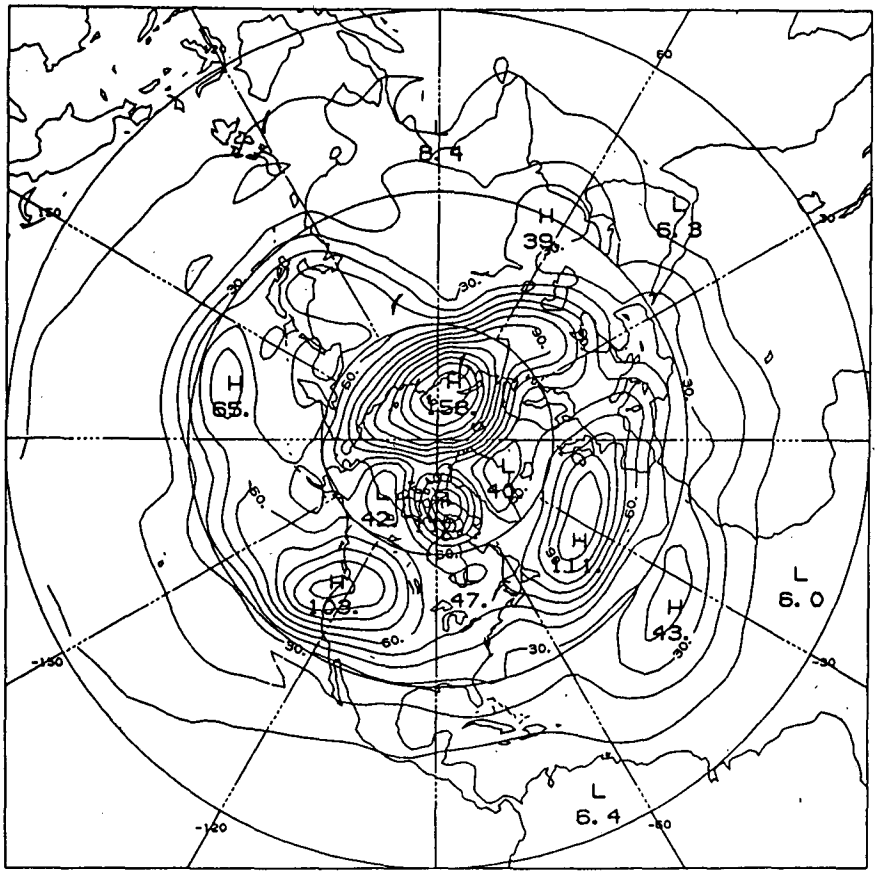

FIG. 5.5a. Simulated low pass filtered RMS of 500 mb height for DJFM. The contour interval is 10 m.

example, the model simulated easterlies in the tropical Pacific north of the equator, and the westerlies over the northern Pacific Ocean are stronger than the analyses, giving rise to a significantly stronger anticyclonic circulation in both seasons (see Figs. 4.15b and 4.16b). The magnitude of the wind error during the summer season is not as large, but neither is the magnitude of the analyzed mean wind itself. The model-simulated westerly winds during summer over Africa, the Arabian Sea and India are stronger than the corresponding analyses. The simulated easterlies over the north tropical Atlantic are far weaker than their analyzed counterparts.

In the seasonal means of the simulations, then, the sea level pressure, winter stationary waves and jet level zonal winds are well simulated. The zonal mean Hadley cell is reasonably close to the analyses. Generally, the winter hemisphere in both simulations is closer to analyses than the summer hemisphere.

5. Simulation of the stationary waves and transients

The stationary wave variance (zonal mean of $\bar{Z}^{*2}$) for the DJFM mean is shown in Fig. 5.1. The first panel (a) represents the simulated value, while the second panel (b) is the value taken from NMC verifying analyses. As may be seen in the analyses, the variance in 1985–86 was 31% higher than climatology at the maximum near the tropopause at 48°N (for an estimate of the climatology, see Shukla et al. 1981). The model result was even higher, exceeding the observed value by 21%.

In the MJJA simulation (Fig. 5.2), the simulated stationary wave variance is also larger than the analyses, and the excess is even larger than in the DJFM simulation. In fact, the stationary wave variance in the MJJA simulation reaches nearly wintertime values, exceeding the analyzed variance by a factor of more than 2 at the maximum in the summer hemisphere at 200 mb. There is a secondary maximum in stationary wave activity near the surface in the subtropics which the model simulates fairly well though it too is overestimated.

Model transient variance in both seasons is a major deficiency in the simulations. In Fig. 5.3, the total root-mean-square transient eddy variance for 500 mb geopotential height is shown. A representation of the seasonal cycle has been removed from the data by means of a least-squares fit to a parabola before this quantity

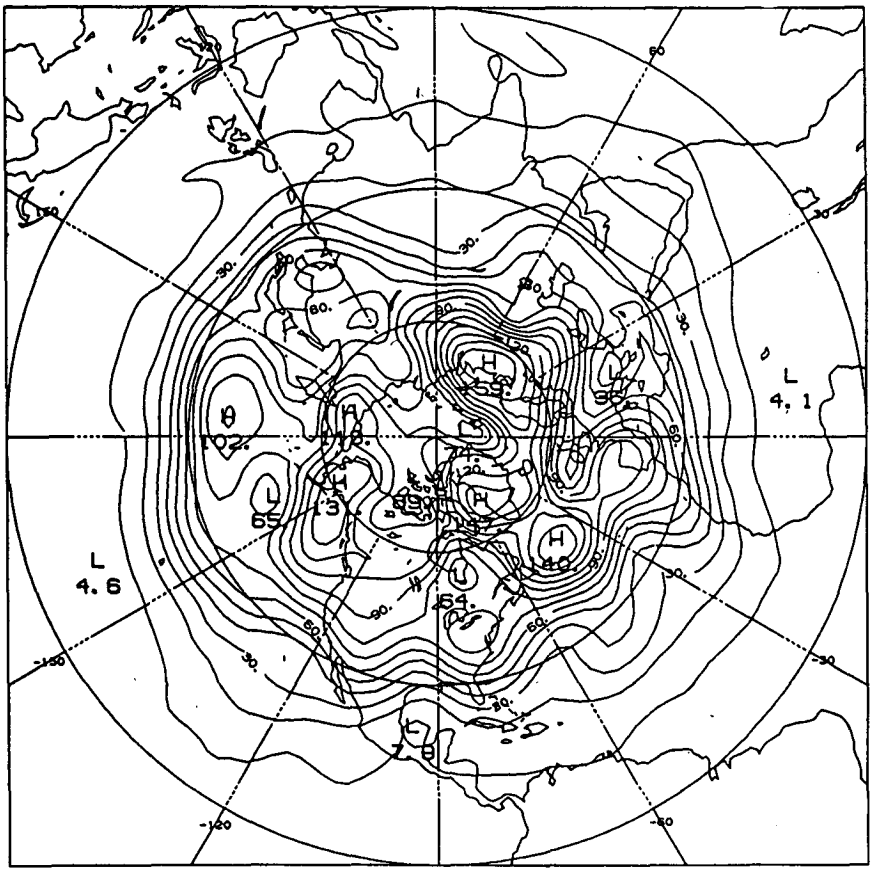

FIG. 5.5b. As in 5.5a except for observed low pass filtered RMS.

was computed. The analyzed variance may be seen to have three maxima: one center over the north central Soviet Union, one over southern Alaska, and a pair of maxima over Iceland and east of Newfoundland. The root-mean-square deviation from the seasonal mean in these three centers ranges from 158 to 183 m. The model variance map shows the same three maxima; however, only the center over the north central Soviet Union is at the analyzed location or of the observed magnitude. The Atlantic Ocean and Pacific Ocean centers are displaced southward of their analyzed positions and are weaker than the analyses. A comparison with the climatological distribution of transient eddy variance reveals that the magnitude of the model variance centers is smaller than the ensemble of 15 winters (Shukla et al. 1981).

The MJJA simulation is similar in this respect. As may be seen in Fig. 5.4b, there are also three major centers of action in the summer months, in the Arctic Ocean north of the central Soviet Union, one west of the Aleutian archipelago and a center south of Iceland. The model missed the center in the Arctic Ocean, split the Aleutian center into two north Pacific centers and produced an unobserved center east of Iceland. The magnitude of transient eddy activity in all these regions was less than the analyses. It should also be noted that the pattern of transient variance in the model has less structure than the analyses.

The smaller than analyzed transient activity is found on several time scales. As shown in Figs. 5.5 and 5.6, the low pass filtered (Blackmon 1976) transient eddy variances in both seasons are smaller than observed and have geographical differences from the analyzed maps of variance. Particularly striking is the difference between the simulated and analyzed DJFM low pass variance in the vicinity of the west coast of North America. The analyzed center over Alaska and the Bering Strait is missing in the model result and an unobserved center is present in the simulation over British Columbia. Figures 5.7 and 5.8 show the band pass filtered transient eddy variance. Here again, the model undersimulates the observed transient activity, particularly in MJJA when the storm tracks are weaker and poleward of their analyzed positions. In this series of figures, the best simulation appears to be the DJFM band pass filtered transience in which the Pacific and

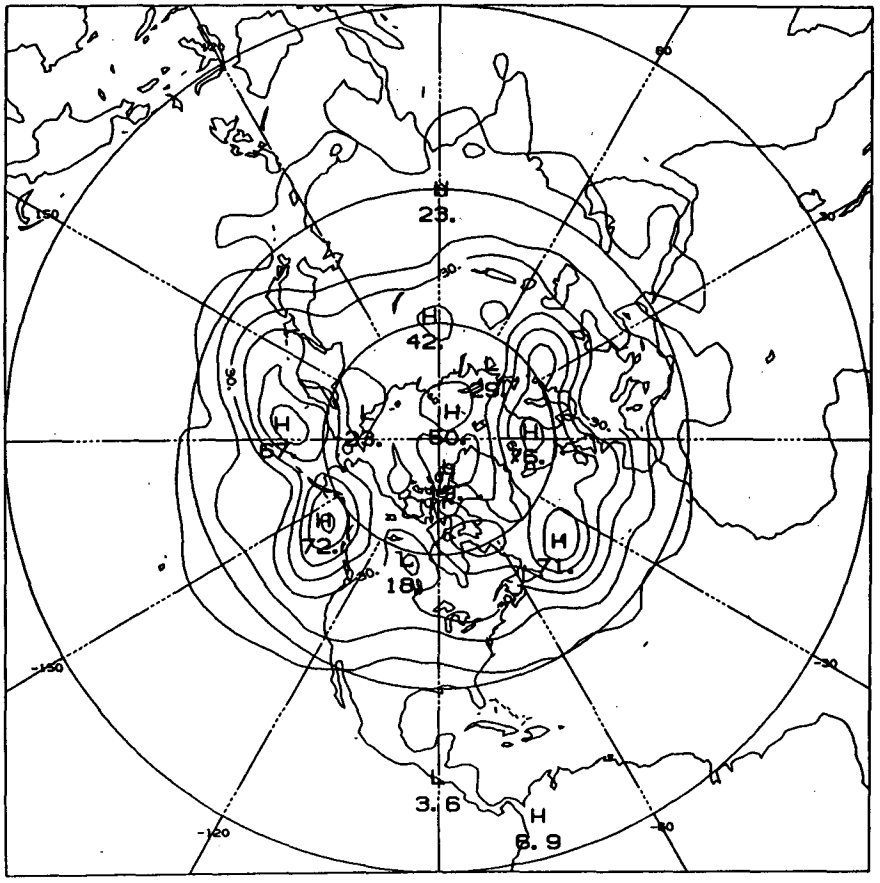

FIG. 5.6a. Simulated low pass filtered RMS of 500 mb height for MJJA. The contour interval is 10 m.

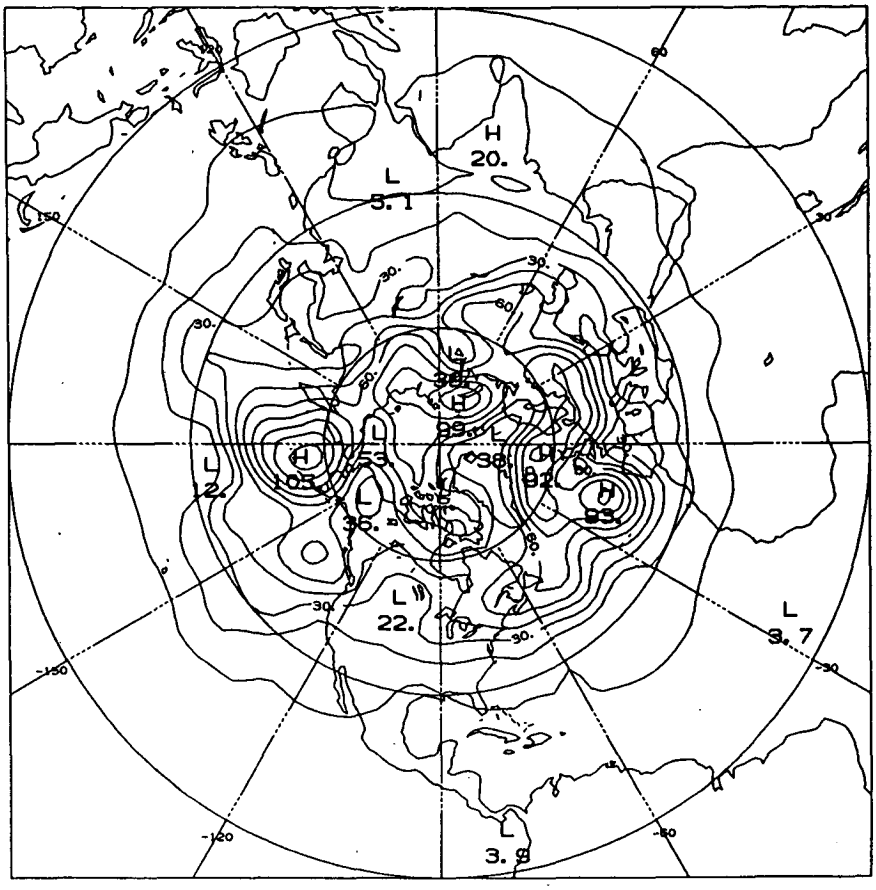

FIG. 5.6b. As in 5.6a except for observed low pass filtered RMS.

Atlantic storm tracks are clearly delineated in both the analyses and the simulation and the magnitude of simulated transience approaches that of the analyses.

6. Model hydrologic cycle and surface fluxes

The mean DJFM precipitation rate in the model is shown in Fig. 6.1a. For comparison, we have shown the observed outgoing longwave radiation Fig. 6.1b (provided by the Climate Analysis Center). It should be noted that the precipitation rate from the model is computed on the Gaussian grid which, at approximately 1.8 deg lat by 2.8 deg long, is a higher resolution than is available for the OLR data (2.5 deg by 2.5 deg). Consequently, for a more faithful comparison, we have applied a nine-point spatial smoothing to the model data. The observed precipitation belts are clearly associated with the Pacific and Atlantic intertropical convergence zones in both figures, and the active convection region in Indonesia is well simulated. However, the simulated rainfall patterns, especially over the tropical land masses, have serious deficiencies. The excessive rainfall over central Saudi Arabia, South Africa and southern South America are not observed, and storm track related precipitation over the western North Pacific is considerably northward of the OLR trough.

In MJJA, the problems over South Africa and South America are also present (Fig. 6.2a), and the precipitation over the Australian desert is greater than twice as much as observed climatologically (see Jaeger 1976). The east Asian monsoon is fairly well simulated in its broad aspects: there are two maxima in rainfall, one over western India and one over Bangladesh, both in agreement with climatology and the OLR minima. One feature that is common to both seasonal simulations is that the model-simulated tropical rain belt is generally north of its observed position. Also, the precipitation rates over oceanic regions are more similar to observational estimates than over continental regions.

The surface sensible heat flux for the DJFM simulation is shown in Fig. 6.3. The distribution of this quantity is similar to that found using the GLAS GCM (Shukla et al. 1981), except east of Greenland and west of Alaska where the NMC model gives significantly weaker and stronger fluxes, respectively. The global mean sensible heat flux in DJFM is 30 W m^{-2}, slightly larger than that found with the GLAS GCM. The

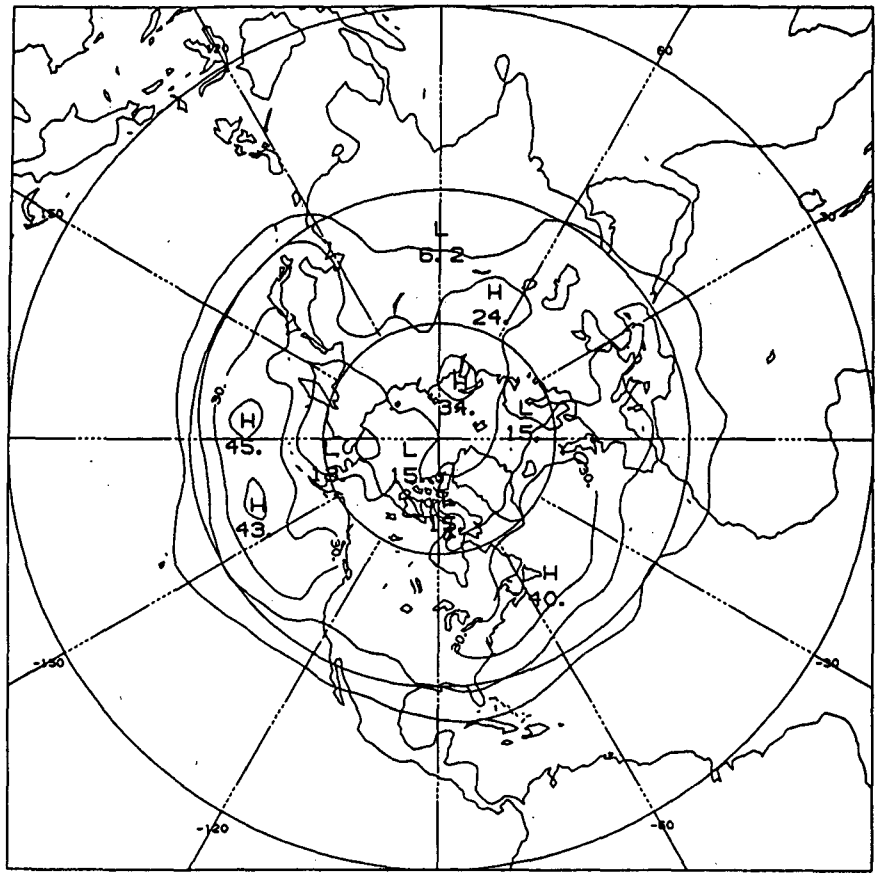

FIG. 5.7a. Simulated band pass filtered RMS of 500 mb height for DJFM. The contour interval is 10 m.

DJFM simulation also compares well, in some respects, with recent observational studies of oceanic surface heat flux (Esbensen and Kushnir 1981). The major centers of heat flux over the warm western boundary currents are simulated, but the flux is larger than observed nearly everywhere, and up to a factor of 2 larger than observed over the Kuroshio. In MJJA, the global mean surface sensible heat flux is 36 W m^{-2}, larger than in DJFM despite the fact that the warm western boundary ocean currents are much more in evidence in the Northern Hemisphere. The MJJA simulation shown in Fig. 6.4 also compares quite closely with that of the GLAS GCM and observations except near the Antarctic sea ice margin where maxima of more than 75 W m^{-2} are produced by the NMC model.

The surface latent heat flux in both DJFM and MJJA (Figs. 6.5 and 6.6) is similar to observational estimates (Schutz and Gates 1971a) with nearly identical patterns and larger magnitudes. The global mean surface latent heat flux in DJFM is 92 W m^{-2} (3.16 mm day^{-1} evaporation) which may be compared with Schutz and Gates' estimate of 3.12 mm day^{-1} for the month of January. The MJJA figure of 104 W m^{-2} or 3.56 mm day^{-1} is 8.5% larger than the observational estimate of 3.28 mm day^{-1} (Schutz and Gates 1971b).

7. Summary, discussion and conclusions

We have integrated the operational medium range forecast model of NMC twice for 110 days in simulations of both the winter and summer global circulations. We found that the time mean circulation is reasonably well simulated by this model, particularly in the sea level pressure and jet level zonal winds in the troposphere. We found agreement between the time mean zonal mean circulation of the model and that of the analyzed atmosphere, but we noted that the model produces a tropical rainfall distribution which is only broadly correlated with the observed. Generally, the model winter hemisphere is a better simulation than the model summer hemisphere.

We have shown that the model is colder than the analyses nearly everywhere in the zonal mean. This cooling may be considered separately in three separate regions: the global tropospheric cooling of 1–5 K, the tropical tropopause cooling of 9–10 K and the polar

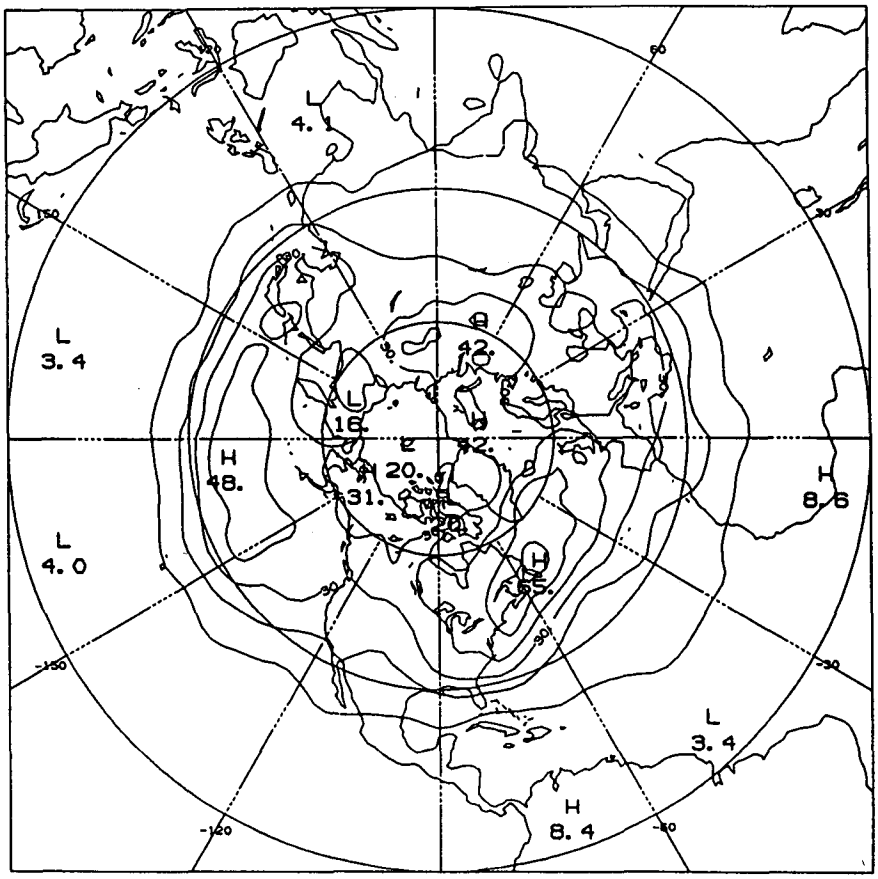

FIG. 5.7b. As in 5.7a except for observed band pass filtered RMS.

stratospheric cooling of 10–18 K. It is our speculation that the global tropospheric cooling may be reduced by altering the radiative properties of the externally prescribed clouds to be more consistent with the remainder of the model's physical parameterizations. The tropical tropopause cooling is probably due to insufficient moisture supply at the cloud base and insufficient convective heating above 300 mb, as suggested by recent experiments at NMC with shallow convection and updated cumulus convection algorithms. The polar stratospheric cooling is a problem which has always plagued GCM integrations and for which we can offer no specific speculation except to suggest that the problem may be ameliorated by the improvement of parameterized heating as suggested above and by the improvement of horizontal and vertical heat flux simulations in experiments suggested below.

The cooling in the lower stratosphere near the poles probably is related to one of the major problems with the zonal mean zonal wind simulation, namely, the poleward shift of the jet cores. The other major feature of the zonal wind error is the tropical easterly bias. We suggest that this is probably indicative of a mean meridional Hadley circulation which is too weak relative to the divergence of eddy zonal momentum flux. Thus, changes in the mean meridional circulation simulation or the simulation of the orientation of the eddies may significantly alter the easterly bias. Note that increasing the convective heating may produce a stronger Hadley cell as well as warming the tropical troposphere, thus reducing the zonal mean zonal wind error through both mechanisms.

In the simulation of stationary eddies, we noted that the summer hemisphere waves were quite wrong, a feature which was particularly noticeable in DJFM. One possible explanation of the difference between the two hemispheres lies in the forcing mechanism of extratropical stationary waves. In the winter hemisphere where the zonal flow is strong, the waves are probably primarily forced by orography, but the summer hemisphere waves are more thermally forced. We have seen that the diabatic heating (precipitation) rate is in poor agreement with estimates of the observed heating rate implying that the thermally forced part of the stationary waves cannot be expected to be correct. It is also implied that the zonal flow is erroneously simulated as discussed above. This hypothesis may be readily examined using a linear model to diagnose the relative

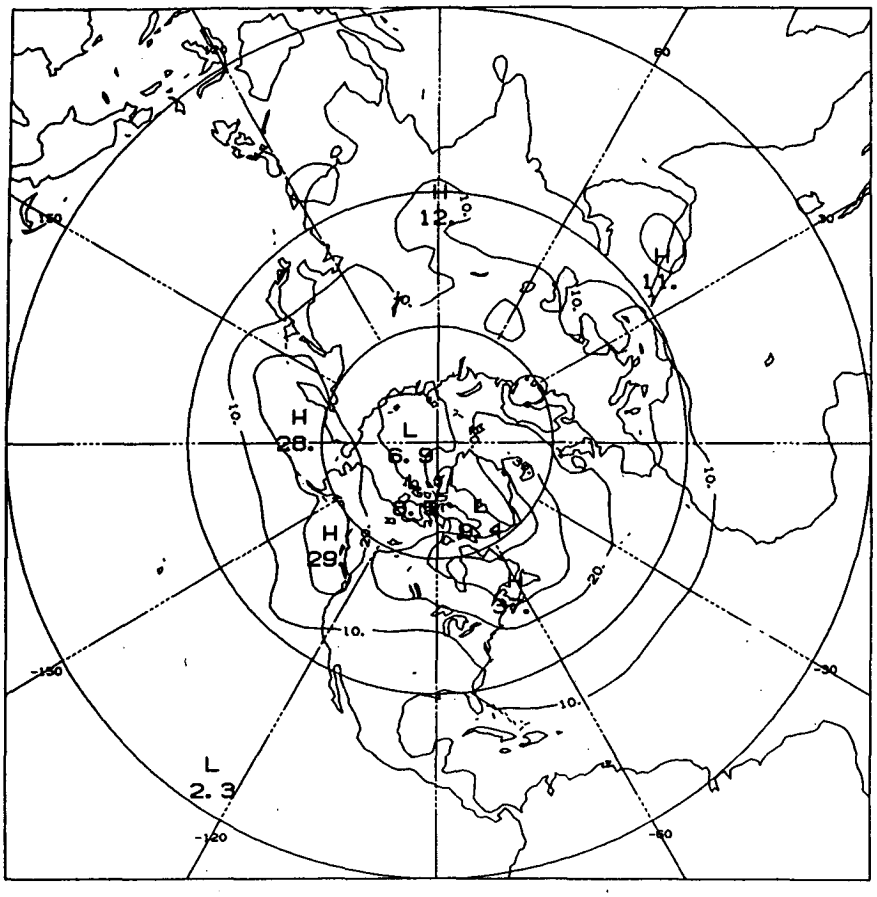

FIG. 5.8a. Simulated band pass filtered RMS of 500 mb height for MJJA. The contour interval is 10 m.

contributions of thermal and orographic forcing to the winter and summer stationary waves in the model.

With regard to the diabatic heating problem, we have indicated that the precipitation rate is more poorly simulated over land than ocean. It is our speculation that this is related to the oversimplified treatment of land surface subgrid-scale processes in the model. A more consistent formulation of momentum, heat and moisture fluxes over a land surface with varying surface roughness and soil and vegetation types is probably needed. We have included maps of the seasonal mean surface fluxes of sensible and latent heat which show these quantities to be considerably different in magnitude from other GCM simulation or observational estimates. While no verification of these results is possible, they have been included with a view toward comparison with future, more accurate surface flux parameterizations. The incorrect features of the precipitation over tropical and subtropical land areas may be responsible for the erroneous shift of the subtropical jet in the Southern Hemisphere, the misplacement and overestimate of stationary wave activity in the summer hemisphere, and individual features of the velocity potential error in both hemispheres.

We found that, in addition to the seasonal mean quantities, the model has difficulties in simulating the transient variance on all subseasonal time scales, including the month-to-month variability of the stationary waves (not shown). We wish to suggest that this transience deficiency is related to the possibility that the stationary waves are phase-locked to the silhouette orography. That is, by enhancing the orography to achieve observed stationary wave amplitudes, we may have reduced the degree to which these quasi-stationary waves may fluctuate on monthly time scales. This is a strong possibility in the low-pass filtered RMS deviations, and the fact that the band-pass filtered RMS deviation errors are correlated with the low-pass errors is suggestive that the storm tracks are affected by the immobility of the stationary eddies. This hypothesis may also be examined in a linear model framework. A more remote possible cause lies in the near absence of zonal variation of the net radiation at the surface. This is due to the fact that the cloudiness is specified and zonally

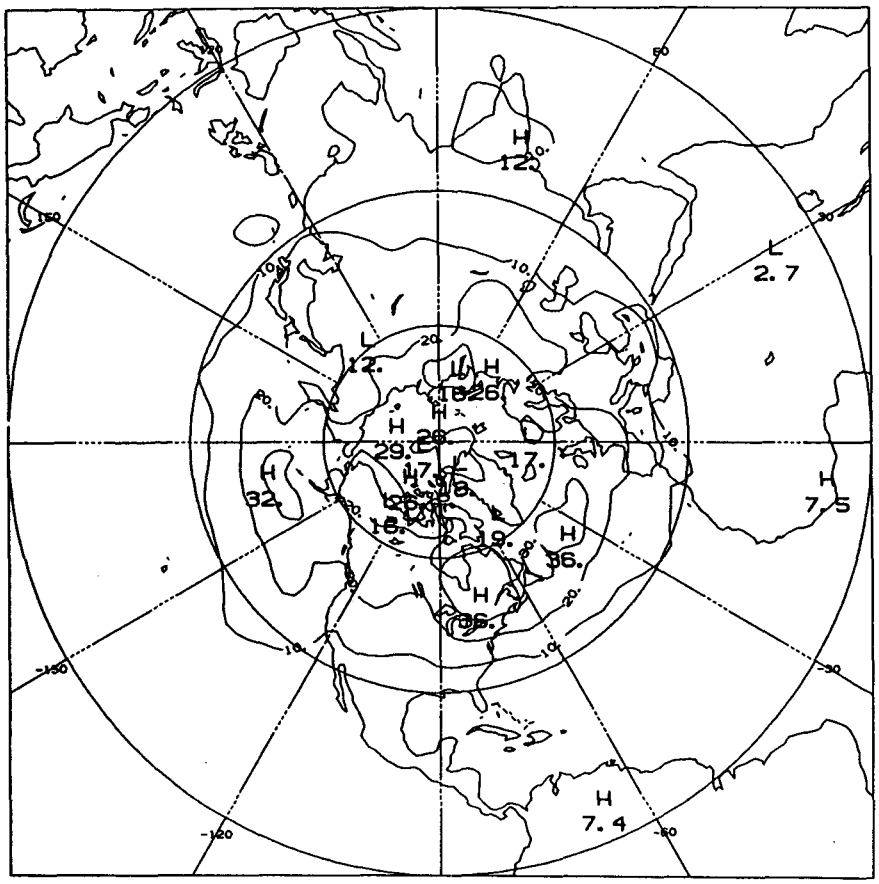

FIG. 5.8b. As in 5.8a except for observed band pass filtered RMS.

symmetric. Testing this conjecture, however, will require more investigation since the cloud radiation interaction can be extremely sensitive.

It is our speculation that the differences between the winter and summer simulations, in terms of their agreement with the observations, are mostly due to the problem with the simulated tropical and summer hemisphere rainfall. This would seem to indicate that improving the tropical rainfall simulation can have a major impact on the simulation of the seasonal cycle as well as the mean components of the winter and summer circulations. Another improvement in the simulations is to be expected by the elimination of the constraint of zonally symmetric fixed cloudiness for the radiative transfer calculation.

Acknowledgments. The preparation, running and postprocessing of a general circulation model constitute an undertaking in which many unseen hands participate. We wish to thank Mr. Eros Albertazzi, Mr. Paul Dirmeyer, Mr. Michael Fennessy, and Mr. Eric Hackert who performed the postprocessing of model output and observations and helped to prepare the figures. We also thank Dr. Piers Sellers who helped to analyze the model results and the remaining members of the Center for Ocean–Land–Atmosphere Interactions whose advice was invaluable. We acknowledge assistance from the members of the Development Division of the National Meteorological Center, especially Dr. Joseph Gerrity, Mr. Robert Kistler, Dr. J. Sela and Dr. Glenn White who were instrumental in helping us to learn the model and in providing codes and data. The generous granting of computer time at NMC as well as a cooperative agreement between COLA and NMC are due to the efforts of Dr. William Bonner for which we are grateful. Suggestions and comments were made by Dr. Eugenia Kalnay, Dr. Kikuro Miyakoda and an anonymous reviewer and we thank them. We also thank Ms. Sharon Busching and Ms. Marlene Schlichtig for expert preparation of this manuscript.

This research was supported under NSF Grant ATM-8414660 and additional computing resources were provided by the National Space and Earth Sciences Computer Center under NASA Grant NAGW-557.

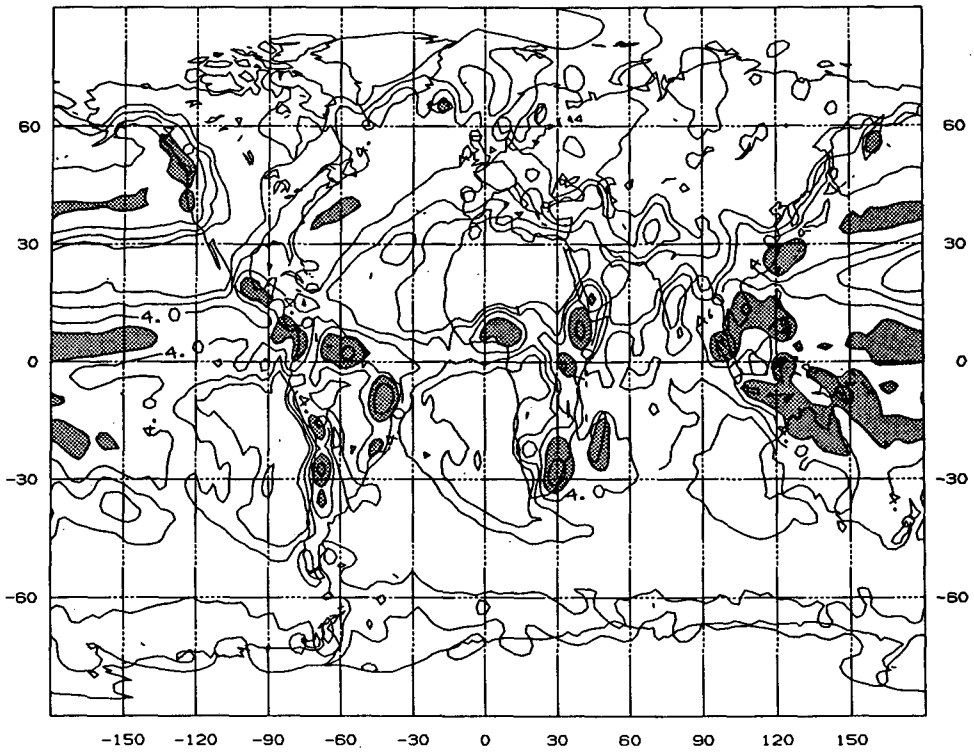

FIG. 6.1a. The DJFM mean of the simulated precipitation rate. Contours are 1, 2, 4, 8, and 16 mm day^{-1}. Shading indicates regions greater than 8 mm day^{-1}.

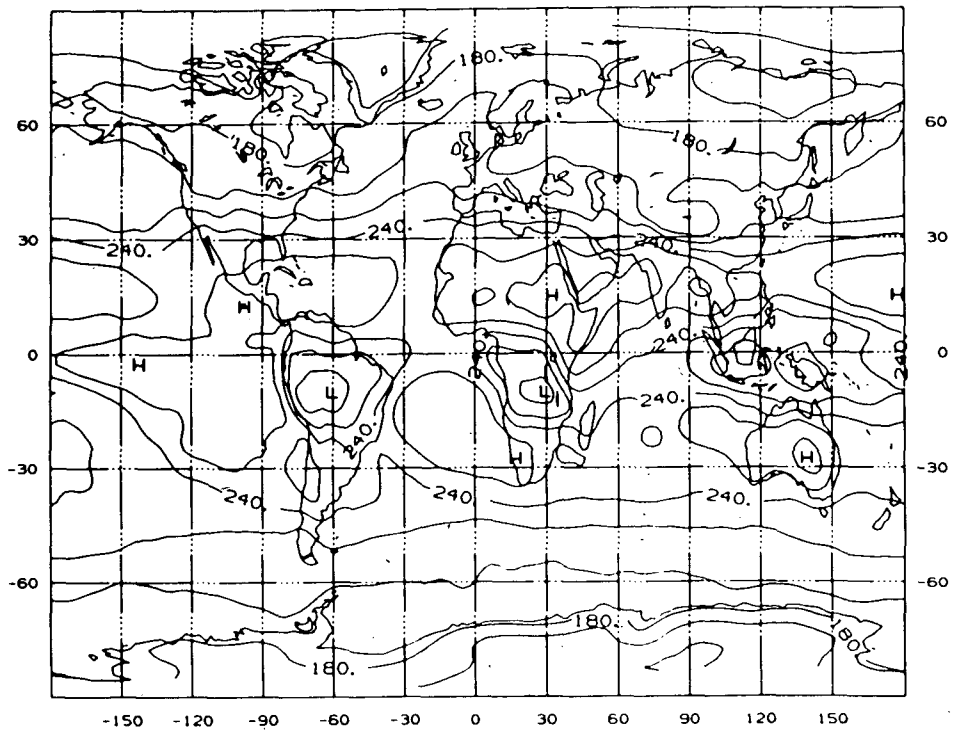

FIG. 6.1b. The DJFM mean of the observed outgoing long wave radiation at the top of the atmosphere. The contour interval is 20 W m^{-2}.

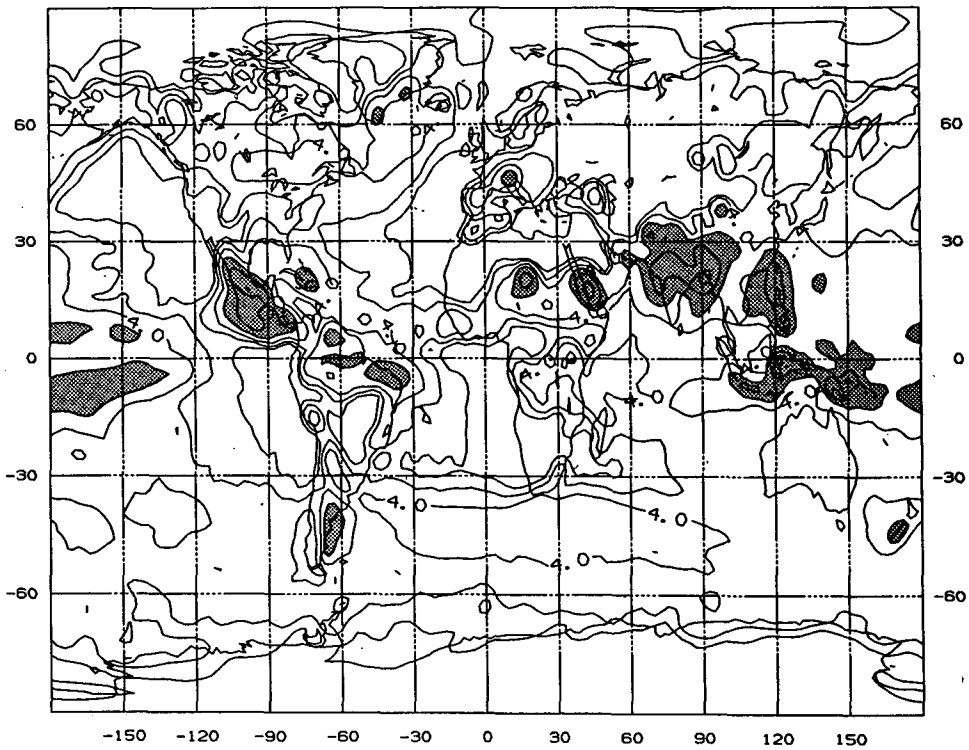

FIG. 6.2a. As in Fig. 6.1a except for MJJA mean.

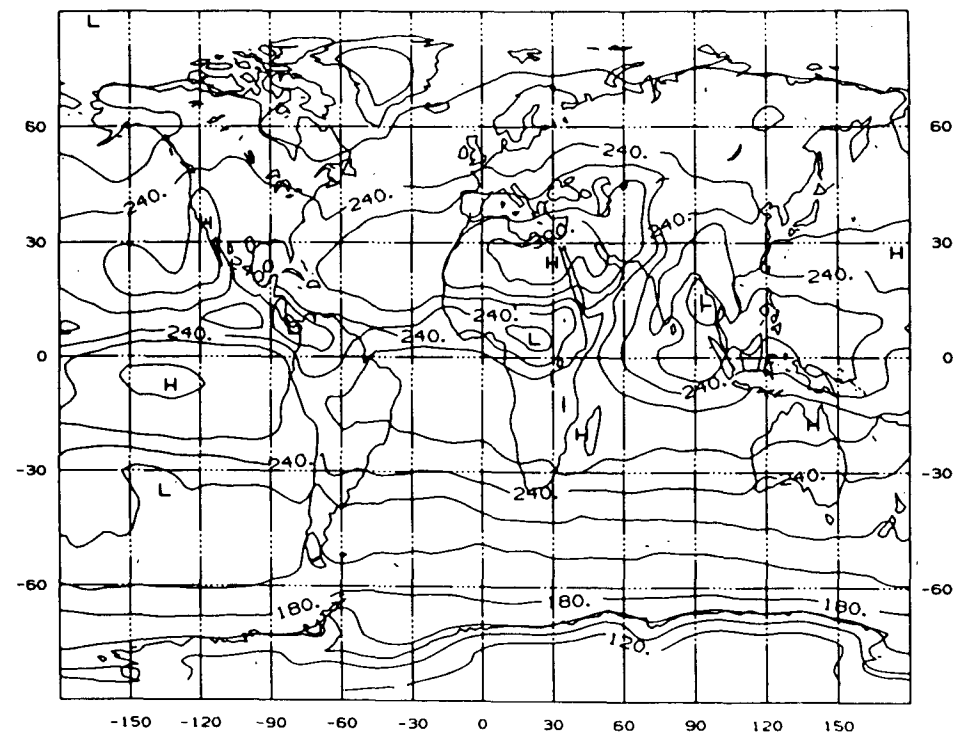

FIG. 6.2b. As in Fig. 6.1b except for MJJA mean.

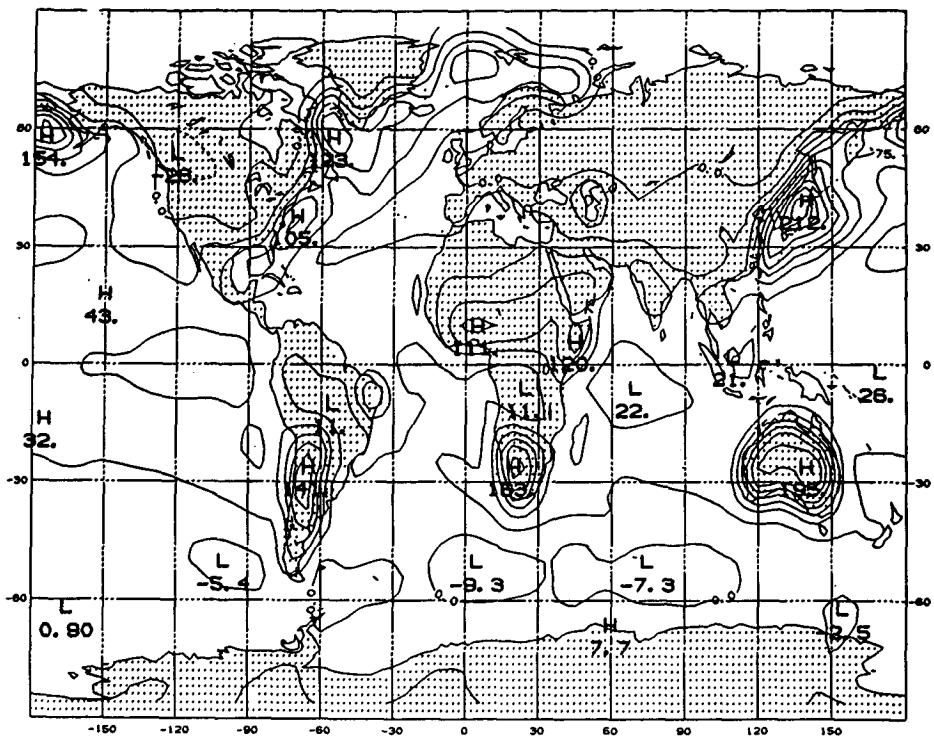

FIG. 6.3. The DJFM mean of the simulated sensible heat flux from the surface into the atmosphere. The contour interval is 25 W m^{-2}.

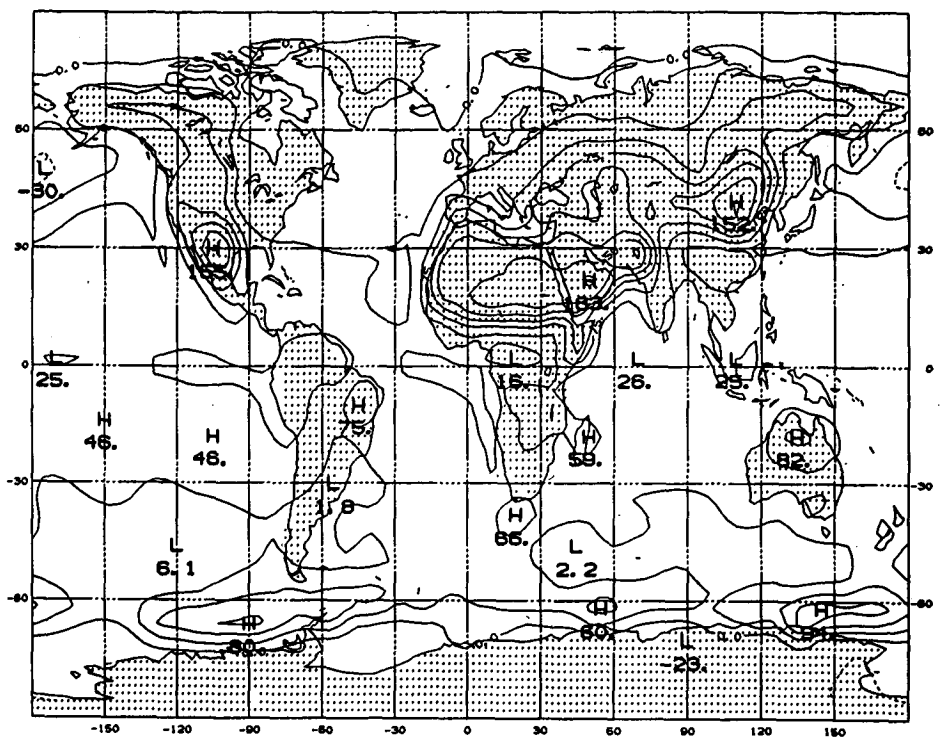

FIG. 6.4. As in Fig. 6.3 except for MJJA mean.

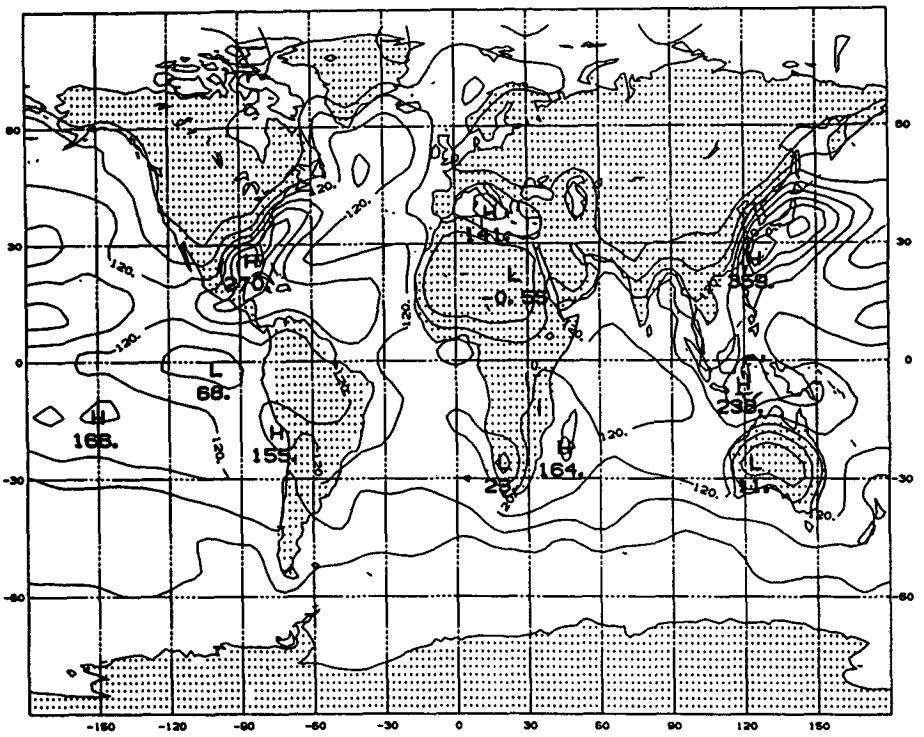

FIG. 6.5. The DJFM mean of the simulated latent heat flux from the surface into the atmosphere. The contour interval is 40 W m^{-2}.

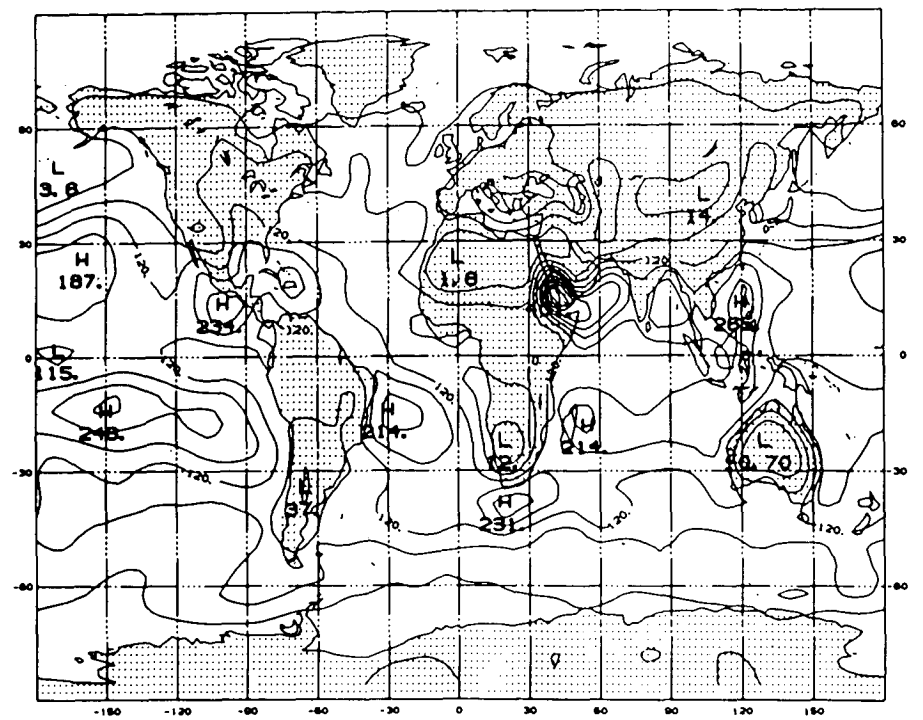

FIG. 6.6. The MJJA mean of the simulated heat flux from the surface into the atmosphere. The contour interval is 40 W m^{-2}.

REFERENCES

Alexander, R. C., and R. L. Mobley, 1976: Monthly average sea-surface temperature and ice-pack limits in a 1° global grid. *Mon. Wea. Rev.*, **104**, 143–148.

British Meteorological Office, 1977: Monthly Ice Charts. Meteorological Office, London Road, Bracknell, Berkshire.

Dey, C. H., and L. L. Morone, 1985: Evolution of the National Meteorological Center Global Data Assimilation System: January, 1982–December, 1983. *Mon. Wea. Rev.*, **113**, 304–318.

Esbensen, S. K., and Y. Kushnir, 1981: The heat budget of the global ocean: An atlas based on estimates from surface marine observations. Climate Research Institute Rep. No. 29, Oregon State University, Corvallis, OR, 239 pp.

Fels, S. B., and M. D. Schwarzkopf, 1975: The simplified exchange approximation: a new method for radiative transfer calculations. *J. Atmos. Sci.*, **32**, 1475–1488.

——, and ——, 1981: An efficient, accurate algorithm for calculating CO_2 15 μm band cooling rates. *J. Geophys. Res.*, **86**, 1205–1232.

Jaeger, L., 1976: Monatskarten des Neiderschlags for die ganze Erde. *Ber. Dtsch. Wetterdienstes*, **18**, No. 139. Im selbstverlag des Deutschen Wetterdienstes, Offenbach, Fed. Rep. Germany.

Kuo, H. L., 1965: On formation and intensification of tropical cyclones through latent heat release by cumulus convection. *J. Atmos. Sci.*, **22**, 40–63.

Lacis, A. A., and J. E. Hansen, 1974: A parameterization for the absorption of solar radiation in the earth's atmosphere. *J. Atmos. Sci.*, **32**, 118–133.

Machenauer, B., 1977: On the dynamics of gravity oscillations in a shallow water model, with applications to normal mode initialization. *Beitr. Phys. Atmos.*, **50**, 253–271.

Manabe, S., 1969: Climate and ocean circulation, I. The atmospheric circulation and the hydrology of the earth's surface. *Mon. Wea. Rev.*, **97**, 739–774.

Miyakoda, K., and J. Sirutis, 1977: Comparative integrations of global spectral models with various parameterized processes of subgrid scale vertical transports. *Beitr. Phys. Atmos.*, **50**, 445–447.

——, and ——, 1986: Manual of the *E*-physics. Available from the authors at Geophysical Fluid Dynamics Laboratory, Princeton University, P.O. Box 308, Princeton, NJ 08542.

Monin, A. S., and A. M. Obukhov, 1954: Basic laws of turbulent mixing in the ground layer of the atmosphere. *Akad. Nauk SSSR Geofiz. Inst. Tr.*, **151**, 163–187.

Orszag, S. A., 1970: Transform methods for calculation of vector coupled sums: Application to the spectral form of the vorticity equations. *J. Atmos. Sci.*, **27**, 890–895.

Phillips, N. A., 1957: A coordinate system having some special advantages for numerical forecasting. *J. Meteor.*, **14**, 184–185.

——, 1979: The nested grid model. NOAA Tech. Rep. NWS-22, 79 pp.

Posey, J. W., and P. F. Clapp, 1965: Global distribution of normal surface albedo. *Geofisica Int.*, **4**, 33–48.

Reynolds, R. W., 1982: A monthly averaged climatology of sea surface temperature. NOAA Tech. Report #NWS-31, 35 pp.

Robert, A., J. Henderson and C. Turnbull, 1972: An implicit time integration scheme for baroclinic models of the atmosphere. *Mon. Wea. Rev.*, **100**, 329–335.

Schutz, C., and W. L. Gates, 1971a: Global climate data for surface, 800 mb and 400 mb: January. R-915-ARPA. Rand Corporation, Santa Monica, CA, 173 pp.

——, and ——, 1971b: Global climate data for surface, 800 mb and 400 mb: July. R-1029-ARPA. Rand Corporation, Santa Monica, CA, 180 pp.

Sela, J. G., 1980: Spectral modeling at the National Meteorological Center. *Mon. Wea. Rev.*, **108**, 1279–1292.

Shukla, J., D. Straus, D. Randall, Y. Sud and L. Marx, 1981: Winter and summer simulations with the GLAS climate model. NASA Tech. Memo. No. 83866. NASA, Goddard Space Flight Center, Greenbelt, MD.

Wilmott, C. J., C. M. Rowe and Y. Mintz, 1985: Climatology of the terrestrial seasonal water cycle. *J. Climatol.*, **5**, 589–606.